MODIS Global Terrestrial Evapotranspiration (ET) Product

(NASA MOD16A2/A3)

Algorithm Theoretical Basis Document

Collection 5

NASA Headquarters

November 20, 2013

Qiaozhen Mu, Maosheng Zhao, Steven W. Running

Numerical Terradynamic Simulation Group

College of Forestry and Conservation

The University of Montana

Missoula, MT 59812

National Aeronautics and Space Administration

Headquarters
Washington, DC 20546-0001

November 20, 2013

Reply to Attn of: SMD/Earth Science Division

Dr. Steven Running and
Dr. Qiaozhen Mu
Numerical Terradynamic Simulation Group
College of Forestry and Conservation
The University of Montana
Missoula, MT 59812

Dear Drs. Running and Mu:

We have completed the evaluation of your Algorithm Theoretical Basis Document (ATBD) entitled "MODIS Global Terrestrial Evapotranspiration (ET) Product (NASA MOD16A2/A3) Algorithm Theoretical Basis Document, Collection 5" (08-ATBD11-0001), submitted to the Science Mission Directorate's Earth Science Division. A peer review panel evaluated your document in terms of its scientific and technical merit, feasibility, potential value of the data product, and readiness for implementation.

I am pleased to inform you that the panel rated the ATBD as "A," which means: the theoretical basis for the algorithm is sound, and the algorithm is ready for coding and production. The panel recommended that you take the next steps toward securing an implementation of this standard product. You can cite this successful ATBD review to provide justification regarding the particular next steps to be taken. If you have any questions regarding the details of the review process related to your ATBD, please contact me at: (202) 358-0245 or Diane.E.Wickland@nasa.gov.

A copy of the panel review summary for your ATBD is enclosed. Also enclosed are copies of all the individual evaluations received from panelists and non-panelist, "mail-in" reviewers.

I would like to extend my personal congratulations to you and your team and wish you well as you move toward the production of this exciting "new" MODIS product. Again, please accept my most abject apologies for the long delay in completing this review.

Sincerely,

Diane E. Wickland

Dr. Diane E. Wickland
Manager, Terrestrial Ecology Program and
Lead, Carbon Cycle and Ecosystems Focus Area
Earth Science Division
Science Mission Directorate

Enclosures

cc:
Science Mission Directorate/Dr. Bontempi
Dr. Maiden
University of Colorado/Dr. King
NASA Goddard Space Flight Center/Dr. Xiong

Table of Contents

History of MOD16 Evapotranspiration

In the original EOS proposal competition in 1989, Dr. Steve Running proposed and was selected as MODIS Science team member responsible for Leaf area index, evapotranspiration and photosynthesis/net primary production, then designated as MOD 15, 16 and 17. At the ATBD review for at-launch products in 1995, NASA decided to give MOD15 LAI/FPAR to Dr. Ranga Myneni to provide a more theoretically based algorithm, and Dr. Running was directed to focus on MOD 17 PSN/NPP for the Terra at-launch data product. MOD 16 ET was not dropped, but was deprioritized. At the EOS recompete in 2003 NASA selected another investigator to build a MOD 16 ET product but this investigation was not renewed in 2007. In the interim Dr. Running and the NTSG group had changed from an energy balance – surface resistance concept to a Penman-Monteith concept, and had greater success building a globally applicable algorithm. Since much of the processing paralleled our MOD 17 product, NTSG tested, then generated initial global ET datasets. In the 2010 renewal competition for the MODIS Science Team, Dr. Running reproposed MOD 16, based on the new algorithm and global ET datasets now developed, and published in refereed journals. Now, with selection of our 2010 renewal proposal complete, we offer the ATBD. This document represents our formal ATBD for establishing this algorithm and dataset as the official MOD 16 Evapotranspiration product.

Abstract

This Algorithm Theoretical Basis Document (ATBD) describes a level 4 MODIS land data product, MOD16, the global 8-day (MOD16A2) and annual (MOD16A3) terrestrial ecosystem Evapotranspiration (ET) dataset at 1-km spatial resolution over the 109.03 Million km^2 global vegetated land areas. The MOD16 algorithm is based on the logic of the Penman-Monteith equation which uses daily meteorological reanalysis data and 8-day remotely sensed vegetation property dynamics from MODIS as inputs.

The MOD16 ET algorithm runs at daily basis and temporally, daily ET is the sum of ET from daytime and night. Vertically, ET is the sum of water vapor fluxes from soil evaporation, wet canopy evaporation and plant transpiration at dry canopy surface. MODIS 8-day FPAR is used as vegetation cover faction to quantify how much surface net radiation is allocated between soil and vegetation; MODIS 8-day albedo and daily surface downward solar radiation and air temperature from daily meteorological reanalysis data are used to calculate surface net radiation and soil heat flux; daily air temperature, vapor pressure deficit (VPD) and relative humidity data, and 8-day MODIS LAI are used to estimate surface stomatal conductance, aerodynamic resistance, wet canopy, soil heat flux and other key environmental variables. MODIS land cover is used to specify the biome type for each pixel, and the biome-dependent constant parameters for the algorithm are saved in a Biome-Property-Lookup-Table (BPLUT). Except for minimum daily air temperature and VPD, which are directly adopted from the existing algorithm of the MODIS global terrestrial gross and net primary production (MODIS GPP/NPP), the BPLUT is tuned largely based on a set of targeted annual ET for each biome derived from MODIS GPP and water use efficiency calculated from eddy flux towers.

The MOD16 ET has been validated with ET measured at eddy flux towers and ET estimated from 232 watersheds. Averaged over 2000-2010, the total global annual ET over the vegetated land surface is 63.4×10^3 km^3, with an average of 569 ± 358 mm yr^{-1}, comparable to the recent global estimates. Similar to other MODIS level 3 or level 4 MODIS land data products, 8-day and monthly MOD16A2 and annual MOD16A3 datasets are saved in 10-degree Sinusoidal HDFEOS tiles. Thanks to the powerful internal compression of HDFEOS, for each year, the size of the MOD16A2 and MOD16A3 together takes about 39GB. Since 2006, there have been 193 users from 30 countries requesting MODIS ET data from us and now MOD16 from 2000 to 2010 are ready and have been released to the public for free download at our ftp site, ftp://ftp.ntsg.umt.edu/pub/MODIS/Mirror/MOD16/ .

Figure Captions

Figure 1 Seven-year mean percentage of MODIS 8-day Leaf Area Index (LAI) period contaminated by unfavorable atmospheric conditions, especially by cloud cover, during growing season, defined as annual NPP quality (Zhao et al., 2005). Similar situation can be applied to MODIS LST, making it impractical to use an energy balance model to calculate ET globally. White colored area in land is barren or inland water.

Figure 2 Flowchart of the improved MOD16 ET algorithm. LAI: leaf area index; FPAR: Fraction of Photosynthetically Active Radiation.

Figure 3 The 8-day composite leaf area index (LAI) in Amazon region for the 8-day period 081 (March 21–28) in 2001 for (a) the original with no temporal interpolation of the LAI and (b) the temporally interpolated LAI.

Figure 4 Distribution of the 46 AmeriFlux eddy flux towers used for validation of the improved ET algorithm. The background is the MOD12Q1 land cover type 2, with the blue color for the water body.

Figure 5 The ET measurements (black dots, OBS), the ET estimates driven by flux tower measured meteorological data (red lines) and GMAO meteorological data (blue lines) over 2000-2006 at seven tower sites, Donaldson (a), LBA Tapajos KM67 Mature Forest (b), Willow Creek (c), Little Prospect Hill (d), Tonzi Ranch (e), Walnut River (f) and Bondville (g).

Figure 6 Comparisons of the average ET observations to the average daily ET estimates with the GMAO parameterized algorithm (a,b) and MERRA GMAO parameterized algorithm (c, d) across all the available days at the 46 flux tower sites. These data were created using (1) tower-specific meteorology (a, c), (2) global GMAO meteorology (b) and MERRA GMAO meteorology (d). The solid red lines represent that the ratio of ET estimates to ET measurements is 1.0 and the solid black lines are the regression of the ET estimates to measurements.

Figure 7 Global annual MOD16 evapotranspiration (top) over 2000-2006 driven by global GMAO (v4.0.0) meteorological data and (bottom) over 2000-2010 driven by global MERRA GMAO meteorological data.

Figure 8 Comparison of the histograms of climatological average of global annual evapotranspiration driven by GMAO meteorological data (red solid line) over 2000-2006 and by MERRA GMAO meteorological data (solid black line) over 2000-2010. The GMAO-driven global average ET is 568.4 mm/yr and 568.7 mm/yr driven by MERRA GMAO meteorology (see text). These comparisons are only for vegetated land surfaces. The vegetated land area is shown as the colored area in Fig. 7.

Figure 9 Climatological zonal mean of global annual evapotranspiration by GMAO meteorological data over 2000-2006.

Figure 10 Spatial pattern of the global MOD16 ET seasonality during 2000-2010.

Figure 11 Spatial pattern of global MODIS ET to PET ratio anomalies during 2000-2009. Large-scale ET/PET negative anomalies were mainly caused by droughts.

Figure 12 (Left) Distribution of the 232 watersheds used for validation of global MOD16 ET data. Each watershed is depicted in yellow. (Right) Comparison of annual pseudo ET observations (ET OBS, precipitation minus stream flow) from the 232 watersheds and the MODIS ET estimates averaged over each watershed over at least five years during 2000-2006. The runoff data for the watersheds were provided by Ke Zhang.

Figure 13 MODIS Sinusoidal "10-degree" tile system. For land data products, there are 317 tiles with land pixels, of which 286 tiles with vegetated pixels located between 60˚S to 80˚N.

Table Captions

Table 1 The Biome Properties Look-Up Table (BPLUT) for MODIS ET. ENF: evergreen needleleaf forest; EBF: evergreen broadleaf forest; DNF: deciduous needleleaf forest; DBF: deciduous broadleaf forest; MF: mixed forest; WL: woody savannas; SV: savannas; CSH: closed shrubland; OSH: open shrubland; Grass: grassland, urban and built-up, barren or sparsely vegetated; Crop: cropland.

Table 1.1 BPLUT using Global Modelling and Assimilation Office (GMAO v. 4.0.0) global reanalysis data as input daily meteorological data.

Table 1.2 BPLUT using Modern Era Retrospective-analysis for Research and Applications of Global Modelling and Assimilation Office (MERRA GMAO) as input daily meteorological data.

Table 2 Other parameter values as used in the improved ET algorithm.

Table 3 Input non-satellite meteorological data, satellite data, and output ET data.

Table 4 The University of Maryland (UMD) landcover classification from MODIS land cover dataset (MOD12Q1) used in the MOD16 Algorithm. The data field name is Land_Cover_Type_2 in the MOD12Q1 data field.

Table 5 The tower names, abbreviations, latitude (lat), longitude (lon), biome types in the parentheses, number of days with valid tower measurements (Days), average daily tower evapotranspiration measurements over all the days with valid values (ET_OBS: mm/day).

Table 6 The tower measured annual GPP, tower measured annual ET summed over all the available days divided by the number of years (≤365 days/year), and WUE calculated from equation (39) averaged over all the towers for each vegetation type; the annual MODIS GPP averaged over each vegetation type; the expected MODIS ET as calculated from equation (40); the actual average annual MODIS ET over each vegetation type. ENF: evergreen needleleaf forest; EBF: evergreen broadleaf forest; DNF: deciduous needleleaf forest; DBF: deciduous broadleaf forest; MF: mixed forest; WL: woody savannas; SV: savannas; CSH: closed shrubland; OSH: open shrubland; Grass: grassland, urban and built-up, barren or sparsely vegetated; Crop: cropland. N/A means that no data is available.

Table 7 The tower abbreviations, average daily tower evapotranspiration (ET) measurements over all the days with valid values (ET_OBS: mm/day); the biases (BIAS: mm/day), mean absolute biases (MAE: mm/day), correlation coefficients (R) and Taylor skill scores (S) of ET estimates relative to tower ET measurements for the 46 AmeriFlux eddy flux towers. 1: tower-driven results; 2: GMAO-driven results.

Table 8. 321 users from 38 countries requesting MODIS ET/PET/LE data over 2006-2012. N: number of users.

1. Introduction

All organisms require water for their survival (Oki and Kanae, 2006). Unlike most other natural resources, water circulates and forms closed hydrological cycles. The terrestrial water cycle is of critical importance to a wide array of Earth system processes. It plays a central role in climate and meteorology, plant community dynamics, and carbon and nutrient biogeochemistry (Vörösmarty et al., 1998). Demand for the world's increasingly scarce water supply is rising rapidly, challenging its availability for food production and putting global food security at risk. Agriculture, upon which a burgeoning population depends for food, is competing with industrial, household, and environmental uses for this scarce water supply (Vörösmarty et al 2010; Rosegrant et al., 2003). The water withdrawals from the renewable freshwater resources include blue water from the surface and groundwater as water resources, and green water from the beneficial evapotranspiration (ET) as a loss from the precipitated water over non-irrigated croplands (Oki and Kanae, 2006). Global climate change will affect precipitation and ET, and hence influence the renewable freshwater resources. ET is the second largest component (after precipitation) of the terrestrial water cycle at the global scale, since ET returns more than 60% of precipitation on land back to the atmosphere (Korzoun et al., 1978; L'vovich and White, 1990) and thereby conveys an important constraint on water availability at the land surface. In addition, ET is an important energy flux since land ET uses up more than half of the total solar energy absorbed by land surfaces (Trenberth et al., 2009). Accurate estimation of ET not only meets the growing competition for the limited water supplies and the need to reduce the cost of the irrigation projects, but also it is essential to projecting potential changes in the global hydrological cycle under different climate change scenarios (Teuling et al. 2009).

This is the Algorithm Theoretical Basis Document (ATBD) of a global MODIS land data product, MODIS ET dataset, which is a NASA-planned Earth Observing System (EOS) dataset, named MOD16 in the MODIS datasets. The global MOD16 ET includes evaporation from wet and moist soil, evaporation from rain water intercepted by the canopy before it reaches the ground, and the transpiration through stomata on plant leaves and stems. The MOD16A2/A3 ET products are produced at the 8-day, monthly and annual intervals. The objectives of this ATBD are: (1) to give a review of the current methods for remotely sensed ET estimates, (2) to describe MODIS ET algorithm, whose logic follows the Penman-Monteith equation, (3) to introduce the required input datasets, daily meteorological reanalysis dataset and 8-day composite MODIS albedo and MODIS vegetation dynamics datasets (FPAR/LAI), (4) to detail how parameters are calibrated based on measurements from eddy flux towers and a mature MODIS global GPP dataset, (5) to show the validation results at eddy flux towers and global watersheds and global MODIS 1-km ET from 2000 to 2010, (6) to detail MOD16 variables, data file format, map projection, file name, and size, and finally (7) to summarize the ATBD.

2. Background

Remote sensing has long been recognized as the most feasible means to provide spatially distributed regional ET information on land surfaces. Remotely sensed data, especially those from polar-orbiting satellites, provide temporally and spatially continuous information over vegetated surfaces useful for regional measurement and monitoring of surface biophysical variables affecting ET, including albedo, biome type and leaf area index (LAI) (Los et al., 2000).

The MODerate Resolution Imaging Spectroradiometer (MODIS) onboard NASA's Terra and Aqua satellites, provide unprecedented global information on vegetation dynamics and surface energy variations (Justice et al., 2002), which can be used for regional and global scale ET estimation in near real-time. Three major types of methods have been developed to estimate ET from remote sensing data: (1) empirical/statistical methods which upscale point measured or estimated ET to large scales with remotely sensed vegetation indices (Nagler et al. 2005; Glenn et al. 2008a, 2008b; Jung et al., 2010); (2) physical models that calculate ET as the residual of surface energy balance (SEB) through remotely sensed thermal infrared data (Bastiaanssen et al., 1998a, 1998b; Su et al., 2002; Overgaard et al., 2006; Bastiaanssen et al. 2005; Allen et al. 2007; Kustas and Anderson 2009); (3) and other physical models such as using the Penman-Monteith logic (Monteith 1965) to calculate ET (Cleugh et al. 2007; Mu et al. 2007, 2009, 2011).

2.1 Energy Partitioning Logic

Energy partitioning at the surface of the earth is governed by the following three coupled equations:

$$H = \rho C_P \frac{T_s - T_a}{r_a} \quad (1)$$

$$\lambda E = \frac{\rho C_p}{\gamma} \frac{e_{sat} - e}{r_a + r_s} \quad (2)$$

$$A' = R_{net} - \Delta S - G = H + \lambda E \quad (3)$$

where H, λE and A' are the fluxes of sensible heat, latent heat and available energy for H and λE; R_{net} is net radiation, G is soil heat flux; ΔS is the heat storage flux. λ is the latent heat of vaporization. ρ is air density, and C_P is the specific heat capacity of air; T_s, T_a are the aerodynamic surface and air temperatures; r_a is the aerodynamic resistance; e_{sat}, e are the water vapour pressure at the evaporating surface and in the air; r_s is the surface resistance to evapotranspiration, which is an effective resistance to evaporation from land surface and transpiration from the plant canopy. The psychrometric constant γ is given by

$$\gamma = C_p \times P_a \times M_a/(\lambda \times M_w) \quad (4)$$

where M_a and M_w are the molecular masses of dry air and wet air and P_a is atmospheric pressure.

2.2 Surface Energy Balance Models

Because remote sensing can provide LST information through thermal spectral bands, SEB- based models were proposed and widely being used. In the early stage of energy-balance-based models, most studies used the high resolution remote sensing data, some data sources are even from airborne sensors or sensor mounted above a site (e.g., Norman et al., 1995; Bastiaanssen et al., 1998a, 1998b). The energy balance models calculate the ET through the residual of the surface absorbed energy as $\lambda E = R_{net} - \Delta S - G - H$.

Despite surface aerodynamic temperature is different from remotely sensed LST, the surface energy balance method (SEB) calculates the flux of sensible heat from Equation **Error! Reference source not found.** by substituting the remotely-sensed radiative surface temperature (LST) for T_s, using the measured air temperature (T_a) and calculating the aerodynamic resistance (R_a) from:

$$r_a = \frac{1}{k^2 U}\left[ln\left(\frac{z-d}{z_{0H}}\right) - \psi_H\left(\frac{z-d}{L}\right)\right]\left[ln\left(\frac{z-d}{z_0}\right) - \psi_M\left(\frac{z-d}{L}\right)\right] \quad (5)$$

In this equation, k is von Karman's constant (0.4); U is wind speed at the reference height z; d is the zero-plane displacement height; z_0, z_{0H} are the roughness lengths for momentum and sensible heat, respectively; and ψ_H, ψ_M are the stability correction functions for momentum and heat which depend on the Monin-Obukhov length L (Kaimal and Finnigan, 1994). λE is then calculated as the residual of the energy balance using Equation **Error! Reference source not found.**.

2.3 Models Using Relationship between Vegetation Index and LST

Another family of method using LST to estimate ET is based on the relationship between vegetation index (VI) and LST. Nemani and Running (1989) showed the utility of a scatterplot of VI-LST on a group of pixels inside a fixed square region in a satellite image. The air temperature, soil and vegetation surface temperature required for ET estimates are obtained through the VI-LST triangle plot for an image window (Nishida 2003a, 2003b). However, Hope et al. (2005) found that the relationship between thermal-IR based LST and NDVI at high-latitudes is opposite to that of mid-latitude regions because arctic tundra ecosystems characterized by permafrost provide a large sink for energy below the ground surface. And the algorithm is too complex and some key biophysical parameters are hard to be parameterized at the global scale. More importantly, the method requires LST and this constrains its application at global scale as detailed below.

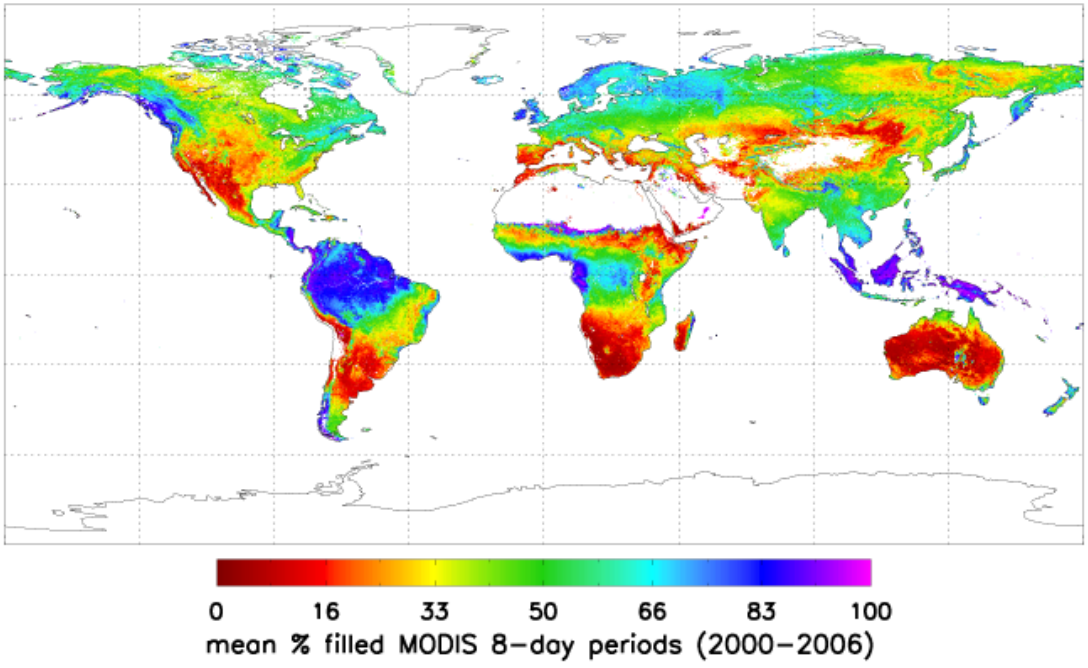

Figure 1 Seven-year mean percentage of MODIS 8-day Leaf Area Index (LAI) period contaminated by unfavorable atmospheric conditions, especially by cloud cover, during growing season, defined as annual NPP quality (Zhao et al., 2005). Similar situation can be applied to MODIS LST, making it impractical to use an energy balance model to calculate ET globally. White colored area in land is barren or inland water.

Both energy-balance-based and VI-LST triangle methods require reliable remotely sensed LST, which makes them impractical to be applied at the global scale. Though we have so far most advanced MODIS sensor and standard 8-day MODIS LST at 1-km resolution, two major reasons restrain the application of energy balance based models at the global scale. First, MODIS LST is the average of cloud-free LST (Wan et al., 2002), and thus an 8-day composite daytime LST may be overestimated at the average overpass time due to exclusion of cloudy days. In regions with high frequency of cloudiness, it is almost impossible to get temporally continuous LST. Figure 1 shows the percentage of missed 8-day MODIS LAI during the growing season due to cloudiness (Zhao et al. 2005), which clearly shows that the frequency of cloud cover at an 8-day interval is considerably high, especially for areas with rain forests and maritime climate. Globally, for vegetated land, the mean percentage of missing 8-day MODIS data due to unfavorable atmospheric conditions is 44.61(±23.65)%, with 38.43% vegetated areas having more than 50% missing 8-days in a growing season (Fig. 1).

Unlike surface contaminated albedo or LAI, which is generally a slow surface variable and can be simply temporally filled with data in adjacent clear sky periods, contaminated LST cannot be simply filled because it is largely influenced by synoptic weather conditions and has large variations. A regional ET estimate using NOAA/AVHRR data over most parts of the central USA has clearly demonstrated that the energy balance model cannot work for areas with cloud cover (Fig. 4 in Mecikalski et al., 1999). Secondly, these LST-required ET algorithms have uncertainties largely due to uncertainties in LST. Zhan et al. (1996) assessed four energy-balance-based ET models and found only one with estimates close to the measured, and models are sensitive to ΔT and other surface parameters. Similarly, Cleugh et al. (2007) compared a surface energy balance model with the Penman-Monteith (hereafter P-M) method (Monteith, 1965), and found that the energy balance model failed because of its sensitivity to small errors in LST. Because of these problems, energy balance models are impractical for application at the global scale in an operational manner. However they often work well within a narrow range of surface conditions for which they were developed and calibrated (e g., Wood et al., 2003; French et al., 2005; Bastiaanssen et al., 2005; Courault et al., 2005; Tasumi et al., 2005; McCabe and Wood, 2006). Courault et al. (2005), Su (2005), and Glenn et al. (2008a) have given excellent reviews of these LST based ET model.

2.4 Penman-Monteith Logic

Another fundamentally different approach to developing a satellite-based evapotranspiration algorithm is the well-known Penman-Monteith (hereafter P-M) equation. Monteith (1965) eliminated surface temperature from Equations (1) – (3) to give:

$$\lambda E = \frac{s \times A' + \rho \times C_p \times (e_{sat} - e)/r_a}{s + \gamma \times (1 + r_s/r_a)} = \frac{s \times A' + \rho \times C_p \times VPD/r_a}{s + \gamma \times (1 + r_s/r_a)} \qquad (6)$$

where $s = d(e_{sat})/dT$, the slope of the curve relating saturated water vapor pressure (e_{sat}) to temperature; A' is available energy partitioned between sensible heat and latent heat fluxes on land surface. $VPD = e_{sat} - e$ is the air vapor pressure deficit. All inputs have been previously defined except for surface resistance r_s, which is an effective resistance accounting for evaporation from the soil surface and transpiration from the plant canopy. The aerodynamic resistance, r_a, can be estimated from Equation (5) using z_{0V} (the roughness length for water vapor) in place of z_{0H} although in practice the two are usually assumed to be equal.

Over extensive, moist surfaces when r_s approaches zero, or when $r_s \ll r_a$, Equation (6) reduces to the equilibrium evapotranspiration rate:

$$\lambda E_{eq} = \frac{s \times A^{'}}{s + \gamma} \qquad (7)$$

which is limited only by available energy. Raupach (2001) demonstrates why (7) is the theoretical upper limit for regional evapotranspiration from land surfaces where moisture availability is not constrained. Conversely when $r_a \ll r_s$, evapotranspiration is largely controlled by the surface resistance and Equation (6) then reduces to:

$$\lambda E_{RS} = \frac{\rho \times C_p \times VPD}{\gamma \times r_s} \qquad (8)$$

The full P-M equation provides a more robust approach to estimating land surface ET because: 1) it combines the main drivers of ET in a theoretically sound way; 2) it provides an energy constraint on the ET rate; 3) modeled ET fluxes are not overly sensitive to any of the inputs, i.e. differentiation of λE shows that (independent) changes in any of the input terms on the right-hand side of Equation 6 yield a conservative change in predicted λE (Thom, 1975 provides a more extensive discussion about the sensitivity of the P-M equation to its inputs); and 4) it has been successfully used to both diagnose and predict land surface ET.

Despite its theoretical appeal, the routine implementation of the P-M equation is often hindered by requiring meteorological forcing data (A', T_a and VPD) and the aerodynamic and surface resistances (r_a and r_s). Radiation and soil heat flux measurements are needed to determine A'; air temperature and humidity to calculate VPD; and wind speed and surface roughness parameters to determine r_a. These problems are not unique to the P-M equation, since A', T_a and r_a are also required by all of the approaches using radiative surface temperature and the surface energy balance to calculate λE, including the resistance-surface energy balance model.

Multi-temporal implementation of the P-M model at regional scales requires routine surface meteorological observations of air temperature, humidity, solar radiation and wind speed. Determining the surface resistance, r_s, is difficult. For a fully closed canopy, where LAI > 3, the surface resistance is the parallel sum of the leaf stomatal resistances, i.e. $r_s = \overline{r_{st}}/\mathrm{LAI}$, where $\overline{r_{st}}$ is the mean stomatal resistance (e.g. Monteith, 1980) which can be measured directly using porometry. Models for estimating maximum stomatal conductance exist (Kelliher et al., 1995) but including the effect of limited soil water availability and stomatal physiology requires either a fully coupled biophysical model such as that by Tuzet et al. (2003) or resorting to the empirical

discount functions of Jarvis (1976), which must be calibrated: neither of these are appropriate for land surface evapotranspiration model that is to be implemented routinely across the globe at kilometre spatial resolution. Determining a *surface* resistance for partial canopy cover is even more challenging with various dual source models proposed (e.g. Shuttleworth and Wallace, 1985) to account for the presence of plants and soil. Given the impediment that r_s presents to using the P-M equation, Cleugh et al. (2007) developed a remotely sensed ET model using a P-M approach driven by MODIS derived vegetation data and daily surface meteorological inputs including incoming solar radiation, surface air temperature and VPD. Stability corrections to r_a (Equation 5) was neglected, although this is justifiable because the P-M equation is relatively insensitive to aerodynamic resistance - especially when $r_a << r_s$ and at daily timescales. Surface albedo and emissivities of the surface and atmosphere needed to determine A', and the aerodynamic roughness needed for r_a, can be derived from remotely sensed radiance data or from models.

Cleugh et al. (2007) used the more theoretically based P-M equation 6 (1965) to estimate ET over Australia with MODIS data. Based on Cleugh et al.'s model (2007), Mu et al. (2007) developed a remotely sensed ET model (RS-ET) to get the first remotely sensed global terrestrial ET map, suggesting it is applicable to operationally estimate global ET in near real time at satellite sensor resolution. Based on Mu et al.'s 2007 RS-ET model, Zhang et al. (2009) developed a model to estimate ET using remotely sensed NDVI data; Yuan et al. (2010) modified Mu et al.'s 2007 RS-ET model by adding the constraint of air temperature to stomatal conductance and calculating the vegetation cover fraction using LAI instead of EVI.

There are also other methods using remote sensing data to estimate global ET. For example, Fisher et al. (2008) used Priestley-Taylor (1972) method to estimate global ET using AVHRR data; Jung et al. (2010) used a machine-learning method to upscale the point FLUXNET tower data to calculate the global ET with remotely sensed data.

In Mu et al.'s RS-ET algorithm (2007), ET was calculated as the sum of the evaporation from moist soil and the transpiration from the vegetation during daytime. Nighttime ET was assumed to be small and negligible. Soil heat flux (G) was assumed to be zero. For daily calculations, G might be ignored (Gavilána et al., 2007). G is a relatively small component of the surface energy budget relative to sensible and latent energy fluxes for most forest and grassland biomes (Ogée et al., 2001; da Rocha et al., 2004; Tanaka et al., 2008) and is generally less than 20% of net incoming radiation for the forest and grassland sites from this investigation (e.g. Weber et al. 2002; Granger, http://www.taiga.net/wolfcreek/Proceedings_04.pdf). However, the assumption of negligible G in RS-ET algorithm is a significant concern for tundra. In the Arctic-Boreal regions, G can be a substantial amount of net radiation, especially early in the growing season. The assumption of a negligible G may be valid in mid-latitude regions on a daily basis, however in these areas a substantial portion of net radiation melts ice in the active layer, especially early in the growing season (Harazono et al., 1995; Engstrom et al., 2006). The RS-ET algorithm neglected the evaporation from the intercepted precipitation from plant canopy. After the event of precipitation, part of the vegetation and soil surface is covered by water. The evaporation from the saturated soil surface is much higher than the evaporation from the unsaturated soil surface, and the evaporation from the intercepted water by canopy is different from canopy transpiration. Mu et al. (2011) have improved the 2007 algorithm by 1) simplifying the calculation of vegetation cover fraction; 2) calculating ET as the sum of daytime and

nighttime components; 3) calculating soil heat flux; 4) improving the methods to estimate stomatal conductance, aerodynamic resistance and boundary layer resistance; 5) separating dry canopy surface from the wet, and hence canopy water loss includes evaporation from the wet canopy surface and transpiration from the dry surface; and 6) dividing soil surface into saturated wet surface and moisture surface, and thus soil evaporation includes potential evaporation from the saturated wet surface and actual evaporation from the moisture surface. This improved ET algorithm is the official MOD16 ET algorithm used to produce the official global terrestrial MOD16 ET product.

3. MOD16 ET Algorithm Descriptions

MOD16 ET algorithm is based on the Penman-Monteith equation (Monteith, 1965) as in equation 6. Figure 2 shows the logic behind the improved MOD16 ET Algorithm for calculating daily MOD16 ET algorithm.

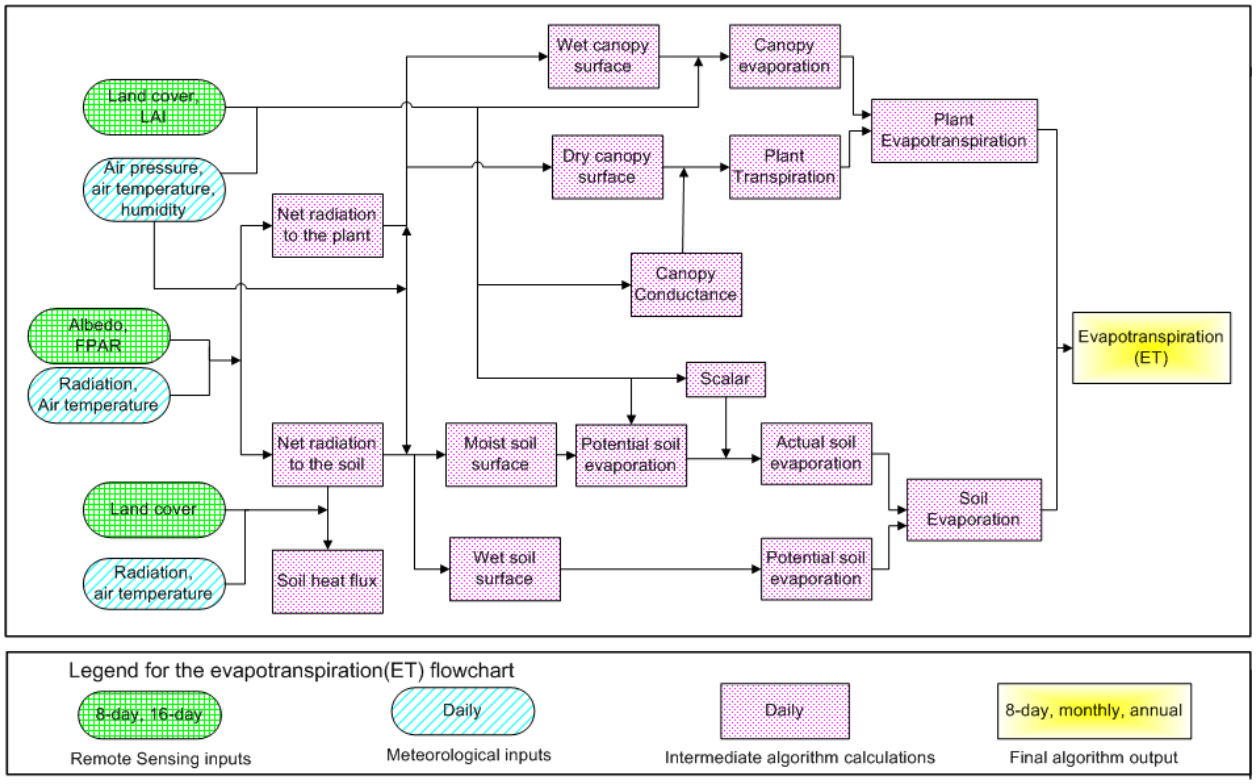

Figure 2 Flowchart of the improved MOD16 ET algorithm. LAI: leaf area index; FPAR: Fraction of Photosynthetically Active Radiation.

3.1 Vegetation Cover Fraction

Net radiation is partitioned between the canopy and soil surface based on vegetation cover fraction (F_C). In the 2007 MOD16 ET algorithm, F_C was calculated as in equation 9 (Mu et al., 2007),

$$F_C = \frac{EVI - EVI_{min}}{EVI_{max} - EVI_{min}} \quad (9)$$

where EVI_{min} and EVI_{max} were the minimum and maximum EVI during the study period, set as constants of 0.95 and 0.05 (Mu et al., 2007), respectively. In the improved algorithm (Mu et al., 2011), to reduce numbers of inputs from MODIS datasets and to simplify the algorithm, we use 8-day 1-km^2 MOD15A2 FPAR (the Fraction of Absorbed Photosynthetically Active Radiation) as a surrogate of vegetation cover fraction (Los et al., 2000),

$$F_C = FPAR \quad (10)$$

3.2 Daytime and Nighttime ET

Daily ET should be the sum of daytime and nighttime ET. To get nighttime average air temperature (T_{night}), we assume that daily average air temperature (T_{avg}) is the average of daytime air temperature (T_{day}) and T_{night}.

$$T_{night} = 2.0 \times T_{avg} - T_{day} \quad (11)$$

The net incoming solar radiation at night is assumed to be zero. Based on the optimization theory, stomata will close at night to prevent water loss when there is no opportunity for carbon gain (Dawson et al., 2007). In the improved ET algorithm, at night, the stomata are assumed to close completely and the plant transpiration through stomata is zero, except for the transpiration through leaf boundary-layer and leaf cuticles (more details in section 3.6). Both nighttime and daytime use the same ET algorithm except that different values at daytime and nighttime are used for the same variable.

3.3 Soil Heat Flux

In MOD16 ET algorithm, the net incoming radiation to the land surface (R_{net}) is calculated as the equations 12 and 13 (Cleugh et al., 2007).

$$R_{net} = (1 - \alpha) \times R_{s\downarrow} + (\varepsilon_a - \varepsilon_s) \times \sigma \times (273.15 + T)^4 \quad (12)$$

$$\varepsilon_a = 1 - 0.26exp^{(-7.77\times10^{-4}\times T^2)}$$

$$\varepsilon_s = 0.97$$

where α is MODIS albedo, $R_{s\downarrow}$ is the downward shortwave radiation, ε_s is surface emissivity, ε_a is atmospheric emissivity, and T is air temperature in °C. At daytime, if R_{net} is less than zero, R_{net} is set to be zero; at nighttime, if R_{net} is less than -0.5 times of daytime R_{net}, nighttime R_{net} is set as -0.5 multiplying daytime R_{net}.

In the improved algorithm, there will be no soil heat flux (G) interaction between the soil and atmosphere if the ground is 100% covered with vegetation. Energy received by soil is the difference between the radiation partitioned on the soil surface and soil heat flux (G).

$$A = R_{net}$$

$$A_C = F_C \times A \quad (13)$$

$$A_{SOIL} = (1 - F_C) \times A - G$$

where A is available energy partitioned between sensible heat, latent heat and soil heat fluxes on land surface; R_{net} is the net incoming radiation received by land surface; A_C is the part of A allocated to the canopy and A_{SOIL} is the part of A partitioned on the soil surface. In 1986, Clothier et al. (1986) proposed a method to estimate soil heat flux using remote sensing data as

$$G_{SOIL} = (0.295 - 0.0133B2/B1) \times A_i \quad (14)$$

where $B1$ and $B2$ are the bandpasses of SPOT filters 610-680 nm, and 790-890 nm, A_i is daytime or nighttime available energy partitioned between latent heat and sensible heat fluxes. Kustas and Daughtry (1990) further improved the method using $B2/B1$ and $NDVI'$.

$$G_{SOIL} = (0.294 - 0.0164B2/B1) \times A_i \quad (15)$$

$$NDVI' = {(B2 - B1)}\Big/{(B1 + B2)}$$

$$G_{SOIL} = (0.325 - 0.208 \times NDVI') \times A_i \quad (16)$$

Daughtry et al. (1990) compared the soil heat flux using different methods with observed data and found that the estimates using $NDVI'$ in equation 16 had the lowest absolute error (13%) with a small positive bias. Jacobsen and Hansen (1999) proposed some other methods to estimate Gsoil as,

$$G_{SOIL} = 4.73 \times T_i - 20.87 \quad (17)$$

$$G_{SOIL} = (-0.27 \times NDVI + 0.39) \times A_i \quad (18)$$

$$G_{SOIL} = (-0.025 \times R_{NIR}/R_{RED} + 0.35) \times A_i \quad (19)$$

where T_i means daytime or nighttime average temperature in °C.

We adopted equations (17) and (18) globally with some constraints. At the extremely hot or cold places or when the difference between daytime and nighttime temperature is low (<5°C), there is no soil heat flux. The soil heat flux is set to be zero in the 2007 version, now it is estimated as

$$Gsoil = \begin{cases} 4.73 \times T_i - 20.87 & T_{\min\_close} \le Tann_{avg} < 25℃, Tday - Tnight \ge 5℃ \\ 0.0 & Tann_{avg} \ge 25℃ \; or \; Tann_{avg} < T_{\min\_close} \; or \; Tday - Tnight < 5℃ \\ 0.39 * A_i & abs(Gsoil) > 0.39 * abs(A_i) \end{cases}$$

$$G = Gsoil \times (1 - F_C) \quad (20)$$

in the improved algorithm, where $Gsoil$ stands for the soil heat flux when $F_C = 0$; $Tann_{avg}$ is annual average daily temperature, and $T_{\min\_close}$ is the threshold value below which the stomata will close completely and halt plant transpiration (Table 1; Running et al., 2004; Mu et al., 2007b; Mu et al., 2011). At daytime, $Gsoil_{day} = 0.0$ if $A_{day} - Gsoil_{day} < 0.0$; at nighttime, $Gsoil_{night} = A_{night} + 0.5 \times A_{day}$ if $A_{day} > 0.0$ and $A_{night} - G_{night} < -0.5 * A_{day}$.

Table 1 The Biome Properties Look-Up Table (BPLUT) for MODIS ET. ENF: evergreen needleleaf forest; EBF: evergreen broadleaf forest; DNF: deciduous needleleaf forest; DBF: deciduous broadleaf forest; MF: mixed forest; WL: woody savannas; SV: savannas; CSH: closed shrubland; OSH: open shrubland; Grass: grassland, urban and built-up, barren or sparsely vegetated; Crop: cropland.

Table 1.1 BPLUT using Global Modelling and Assimilation Office (GMAO v. 4.0.0) global reanalysis data as input daily meteorological data.

PARAMETER	***ENF***	***EBF***	***DNF***	***DBF***	***MF***	***CSH***
T_{min_open} (°C)	8.31	9.09	10.44	9.94	9.50	8.61
T_{min_close} (°C)	-8.00	-8.00	-8.00	-6.00	-7.00	-8.00
VPD_{close} (Pa)	3000	4000	3500	2900	2900	4300
VPD_{open} (Pa)	650	1000	650	650	650	650
gl_sh (m s^{-1})	0.04	0.01	0.04	0.01	0.04	0.04
gl_e_wv (m s^{-1})	0.04	0.01	0.04	0.01	0.04	0.04
Cl (m/s)	0.0032	0.0025	0.0032	0.0028	0.0025	0.0065
RBL_MIN (s m^{-1})	65.0	70.0	65.0	65.0	65.0	20.0
RBL_MAX (s m^{-1})	95.0	100.0	95.0	100.0	95.0	55.0

PARAMETER	***OSH***	**WL**	***SV***	***Grass***	**Crop**
T_{min_open} (°C)	8.80	11.39	11.39	12.02	12.02
T_{min_close} (°C)	-8.00	-8.00	-8.00	-8.00	-8.00
VPD_{close} (Pa)	4400	3500	3600	4200	4500
VPD_{open} (Pa)	650	650	650	650	650
gl_sh (m s^{-1})	0.04	0.08	0.08	0.02	0.02
gl_e_wv (m s^{-1})	0.04	0.08	0.08	0.02	0.02
Cl (m/s)	0.0065	0.0065	0.0065	0.0070	0.0070
RBL_MIN (s m^{-1})	20.0	25.0	25.0	20.0	20.0
RBL_MAX (s m^{-1})	55.0	45.0	45.0	50.0	50.0

Table 1.2 BPLUT using Modern Era Retrospective-analysis for Research and Applications of Global Modelling and Assimilation Office (MERRA GMAO) as input daily meteorological data.

PARAMETER	***ENF***	***EBF***	***DNF***	***DBF***	***MF***	***CSH***
T_{min_open} (°C)	8.31	9.09	10.44	9.94	9.50	8.61
T_{min_close} (°C)	-8.00	-8.00	-8.00	-6.00	-7.00	-8.00
VPD_{close} (Pa)	3000	4000	3500	2900	2900	4300
VPD_{open} (Pa)	650	1000	650	650	650	650

gl_sh ($m\ s^{-1}$)	0.04	0.01	0.04	0.01	0.04	0.04
gl_e_wv ($m\ s^{-1}$)	0.04	0.01	0.04	0.01	0.04	0.04
Cl (m/s)	0.0032	0.0032	0.0032	0.0032	0.0024	0.0065
RBL_MIN ($s\ m^{-1}$)	65.0	65.0	65.0	65.0	65.0	20.0
RBL_MAX ($s\ m^{-1}$)	95.0	95.0	95.0	95.0	95.0	45.0

PARAMETER	***OSH***	**WL**	***SV***	***Grass***	**Crop**
T_{min_open} (°C)	8.80	11.39	11.39	12.02	12.02
T_{min_close} (°C)	-8.00	-8.00	-8.00	-8.00	-8.00
VPD_{close} (Pa)	4400	3500	3600	4200	4500
VPD_{open} (Pa)	650	650	650	650	650
gl_sh ($m\ s^{-1}$)	0.04	0.08	0.08	0.02	0.02
gl_e_wv ($m\ s^{-1}$)	0.04	0.08	0.08	0.02	0.02
Cl (m/s)	0.0065	0.0070	0.0070	0.0075	0.0075
RBL_MIN ($s\ m^{-1}$)	20.0	15.0	15.0	15.0	15.0
RBL_MAX ($s\ m^{-1}$)	45.0	45.0	45.0	45.0	45.0

3.4 Wet Surface Fraction

In the 2007 MOD16 ET algorithm, there was no difference between the ET on the saturated and moist bare soil surface, and there was no evaporation but transpiration on the canopy surface (Figure 1 in Mu et al., 2007). In the improved ET algorithm (Mu et al., 2011), ET is the sum of water lost to the atmosphere from the soil surface through evaporation, canopy evaporation from the water intercepted by the canopy, and transpiration from plant tissues (Fig. 2). The land surface is covered by the plant and the bare soil surface, and percentage of the two components is determined by F_C. Both the canopy and the soil surface are partly covered by water under certain conditions. The water cover fraction ($Fwet$) is taken from the Fisher et al. (2008) ET model, modified to be constrained to zero when relative humidity (RH) is less than 70%:

$$Fwet = \begin{cases} 0.0 & RH < 70\% \\ RH^4 & 70\% \le RH \le 100\% \end{cases} \quad (21)$$

where RH is relative humidity (Fisher et al, 2008). When RH is less than 70%, 0% of the surface is covered by water. For the wet canopy and wet soil surface, the water evaporation is calculated as the potential evaporation as described in sections 3.5 and 3.7.

3.5 Evaporation from Wet Canopy Surface

Evaporation of precipitation intercepted by the canopy accounts for a substantial amount of upward water flux in ecosystems with high LAI. For the improved algorithm, when the vegetation is covered with water (i.e., $Fwet$ is not zero), water evaporation from the wet canopy surface will occur. ET from the vegetation consists of the evaporation from the wet canopy surface and transpiration from plant tissue, whose rates are regulated by aerodynamics resistance and surface resistance.

The aerodynamic resistance ($rhrc$, s m^{-1}) and wet canopy resistance (rvc, s m^{-1}) to evaporated water on the wet canopy surface are calculated as

$$rhc = \frac{1.0}{gl\_sh \times LAI \times Fwet}$$

$$rrc = \frac{\rho \times C_p}{4.0 \times \sigma \times (T_i + 273.15)^3} \qquad (22)$$

$$rhrc = \frac{rhc \times rrc}{rhc + rrc}$$

$$rvc = \frac{1.0}{gl\_e\_wv \times LAI \times Fwet}$$

where *rhc* (s m^{-1}) is the wet canopy resistance to sensible heat, *rrc* (s m^{-1}) is the resistance to radiative heat transfer through air; *gl_sh* (s m^{-1}) is leaf conductance to sensible heat per unit LAI, *gl_e_wv* (m s^{-1}) is leaf conductance to evaporated water vapor per unit LAI, σ (W m^{-2} K^{-4}) is Stefan-Boltzmann constant. Following Biome-BGC model (Thornton, 1998) with revision to account for wet canopy, the evaporation on wet canopy surface is calculated as

$$\lambda E_{wet\_C} = \frac{(s \times A_C + \rho \times C_p \times (e_{sat} - e) \times F_C / rhrc) \times Fwet}{s + \frac{P_a \times C_p \times rvc}{\lambda \times \varepsilon \times rhrc}} \qquad (23)$$

where the resistance to latent heat transfer (*rvc*) is the sum of aerodynamic resistance (*rhrc*) and surface resistance (r_s) in equation 6.

3.6 Plant Transpiration

3.6.1 Surface Conductance to Transpiration

Plant transpiration occurs not only during daytime but also at nighttime. Since most of the transpiration occurs at daytime, the nighttime transpiration was neglected in the 2007 algorithm. In the improved algorithm, both the daytime and night time transpiration are included for the calculation of transpiration.

For many plant species, stomatal conductance (*Cs*) decreases as vapor pressure deficit (VPD) increases, and stomatal conductance is further limited by both low and high temperatures (Jarvis, 1976; Sandford et al., 1986; Kawamitsu et al., 1993; Schulze et al., 1994; Leuning, 1995; Marsden et al., 1996; Dang et al., 1997; Oren et al., 1999, 2001; Xu et al., 2003; Misson et al., 2004). VPD is calculated as the difference between saturated air vapor pressure, as determined from air temperature (Murray, 1967), and actual air vapor pressure. Because high temperatures are often accompanied by high VPDs, we have only added constraints on stomatal conductance for VPD and minimum air temperature, ignoring constraints resulting from high temperature. For the daytime plant transpiration, the stomatal conductance estimation has been improved. In the

2007 algorithm, surface conductance (C_C) was estimated by using LAI to scale stomatal conductance (C_S) from leaf level up to canopy level (Landsberg and Gower, 1997),

$$C_S = C_L \times m(Tmin) \times m(VPD)$$

$$C_C = C_S \times LAI \quad (24)$$

where C_L is the mean potential stomatal conductance per unit leaf area, $m(T_{min})$ is a multiplier that limits potential stomatal conductance by minimum air temperatures (T_{min}), and $m(VPD)$ is a multiplier used to reduce the potential stomatal conductance when VPD (difference between e_{sat} and e) is high enough to reduce canopy conductance (Mu et al., 2007; Zhao et al., 2005). In the case of plant transpiration, surface conductance is equivalent to the canopy conductance (C_C), and hence surface resistance (r_s) is the inverse of canopy conductance (C_C). We calculate the constraints from minimum air temperature (T_{min}) and VPD as:

$$m(T_{min}) = \begin{cases} 1.0 & T_{min} \geq T_{\min\_open} \\ \dfrac{T_{min} - T_{\min\_close}}{T_{\min\_open} - T_{\min\_close}} & T_{\min\_close} < T_{min} < T_{\min\_open} \\ 0.0 & T_{min} \leq T_{\min\_close} \end{cases} \quad (25)$$

$$m(VPD) = \begin{cases} 1.0 & VPD \leq VPD_{open} \\ \dfrac{VPD_{close} - VPD}{VPD_{close} - VPD_{open}} & VPD_{open} < VPD < VPD_{\text{close}} \\ 0.0 & VPD \geq VPD_{close} \end{cases}$$

where *close* indicates nearly complete inhibition (full stomatal closure) due to low T_{min} and high VPD, and *open* indicates no inhibition to transpiration (Table 1). When T_{min} is lower than the threshold value T_{min_close}, or VPD is higher than the threshold VPD_{close}, the strong stresses from temperature or water availability will cause stomata to close completely, halting plant transpiration. On the other hand, when T_{min} is higher than T_{min_open}, and VPD is lower than VPD_{open}, there will be no temperature or water stress on transpiration. For T_{min} and VPD falling into the range of the upper and low limits, the corresponding multiplier will be within 0.0 to 1.0, implying a partial stomatal closure. The multipliers range linearly from 0 (total inhibition, limiting r_s) to 1 (no inhibition) for the range of biomes are listed in a Biome Properties Look-Up Table (BPLUT) (Table 1) (Mu et al., 2007; 2011). Complete details on the derivation of the algorithm and the values used in the BPLUT can be found in section 5. The effect of soil water availability is not included in the ET algorithm. Some studies have suggested that atmospheric conditions reflect surface parameters (Bouchet, 1963; Morton, 1983), and VPD can be used as an indicator of environment water stress (Running et al., 1988; Granger et al., 1989). In addition, Mu et al. (2007b) found that VPD alone can capture interannual variability of the full water stress from both the atmosphere and soil for almost all of China and the conterminous U.S., though it may fail to capture the full seasonal water stress in dry regions experiencing strong summer monsoons.

In the 2007 algorithm, C_L was a constant for all biome types. In the improved algorithm, C_L is set differently for different biomes as shown in Table 1 (Kelliher et al., 1995; Schulze et al., 1994; White et al., 2000). In the improved algorithm, the way to calculate C_C has been revised. Canopy conductance to transpired water vapor per unit LAI is derived from stomatal and cuticular conductances in parallel with each other, and both in series with leaf boundary layer conductance (Thornton, 1998; Running & Kimball, 2005).

$$r_{corr} = \frac{1.0}{\frac{101300}{P_a} \times \left(\frac{T_i + 273.15}{293.15}\right)^{1.75}}$$

$$G_{S\_day}1 = C_L \times m(Tmin) \times m(VPD) \times r_{corr}$$

$$G_{S\_night}1 = 0.0$$

$$G_{CU} = g\_cu \times r_{corr}$$

$$G_S2 = gl\_sh \qquad (26)$$

$$C_{C\_i} = \begin{cases} \frac{G_S2 \times \left(G_{S\_i}1 + G_{CU}\right)}{G_{S\_i}1 + G_S2 + G_{CU}} \times LAI \times (1.0 - Fwet) & (LAI > 0.0, (1.0 - Fwet) > 0.0) \\ 0.0 & (LAI = 0.0, (1.0 - Fwet) = 0.0) \end{cases}$$

$$r_{s\_i} = {}^1/_{C_{C\_i}}$$

where the subscript *i* means the variable value at daytime and nighttime; $G_{S\_day}1$ and $G_{S\_night}1$ are daytime and nighttime stomatal conductance, respectively; G_{CU} is leaf cuticular conductance; G_S2 is leaf boundary-layer conductance; *g_cu* is cuticular conductance per unit LAI, set as a constant value of 0.00001 (m s^{-1}) for all biomes; *gl_sh* is leaf conductance to sensible heat per unit LAI, which is a constant value for each given biome (Table 1). The reason to use the correction function $r_{corr}$is that, the conductance through air varies with the air temperature and pressure. The prescribed values are assumed to be given for standard conditions of 20˚C and 101300Pa. Based on the prescribed daily air temperature (converted to Kelvins) and an air pressure estimated from a prescribed elevation, the prescribed standard conductances are converted to actual conductances for the day according to Jones (1992) and Thornton (1998). r_s is the dry canopy surface resistance to transpiration from the plant. Instead of setting the atmospheric pressure (P_a) as a constant value as in the 2007 algorithm, P_a is calculated as a function of the elevation (*Elev*) (Thornton, 1998).

$$t_1 = 1.0 - \frac{LR_{STD} \times Elev}{T_{STD}}$$

$$t_2 = \frac{G_{STD}}{LR_{STD} \times \frac{RR}{MA}} \qquad (27)$$

$$P_a = P_{STD} \times {t_1}^{t_2}$$

where LR_{STD}, T_{STD}, G_{STD}, RR, MA and P_{STD} are constant values as listed in Table 2. LR_{STD} (K m^{-1}) is standard temperature lapse rate; T_{STD} (K) is standard temperature at 0.0 m elevation; G_{STD} (m s^{-2}) is standard gravitational acceleration; RR (m^3 Pa mol^{-1} K^{-1}) is gas law constant; MA (kg mol^{-1}) is molecular weight of air and P_{STD} (Pa) is standard pressure at 0.0 m elevation.

Table 2 Other parameter values as used in the improved ET algorithm

LR_{STD} (K m^{-1})	T_{STD} (K)	G_{STD} (m s^{-2})	RR (m^3 Pa mol^{-1} K^{-1})	MA (kg mol^{-1})	P_{STD} (Pa)
0.0065	288.15	9.80665	8.3143	28.9644e-3	101325.0

Based on the optimization theory, stomata will close at night to prevent water loss when there is no opportunity for carbon gain (Dawson et al., 2007). In the improved ET algorithm, the stomata are assumed to close completely at night, resulting in $G_S1 = 0.0$.

3.6.2 Aerodynamic Resistance

The transfer of heat and water vapor from the dry canopy surface into the air above the canopy is determined by the aerodynamic resistance(r_a), which was a constant of 20 s m^{-1} in the 2007 algorithm. In the improved algorithm, r_a is calculated as a parallel resistance to convective (rh) and radiative (rr) heat transfer following Biome-BGC model (Thornton, 1998),

$$r_a = \frac{rh \times rr}{rh + rr}$$

$$rh = \frac{1.0}{gl\_bl} \qquad (28)$$

$$rr = \frac{\rho \times C_p}{4.0 \times \sigma \times (T_i + 273.15)^3}$$

where gl_bl (m s^{-1}) is leaf-scale boundary layer conductance, whose value is equal to leaf conductance to sensible heat per unit LAI (gl_sh (m s^{-1}) as in section 3.5), and σ (W m^{-2} K^{-4}) is Stefan-Boltzmann constant.

3.6.3 Plant Transpiration

Finally, the plant transpiration (λE_{trans}) is calculated as

$$\lambda E_{trans} = \frac{(s \times A_C + \rho \times C_p \times (e_{sat} - e) \times F_C / r_a) \times (1 - Fwet)}{s + \gamma \times (1 + r_s / r_a)} \qquad (29)$$

where $r_a$is the aerodynamic resistance calculated from equation 6.

In addition, to monitor environmental water stresses and droughts, we also calculate potential surface ET (see section 3.8). The potential plant transpiration (λE_{POT_trans}) is calculated following the Priestley-Taylor method (1972).

$$\lambda E_{POT\_trans} = \frac{\alpha \times s \times A_C \times (1 - Fwet)}{s + \gamma} \quad (30)$$

$\alpha = 1.26$

3.7 Evaporation from Soil Surface

The soil surface is divided into the saturated surface covered with water and the moist surface by *Fwet*. The soil evaporation includes the potential evaporation from the saturated soil surface and evaporation from the moist soil surface. The total aerodynamic resistance to vapor transport (r_{tot}) is the sum of surface resistance (r_s) and the aerodynamic resistance for vapor transport (r_v) such that $r_{tot} = r_v + r_s$ (van de Griend, 1994; Mu et al., 2007). In the 2007 algorithm, a constant r_{totc} (107 s m^{-1}) for r_{tot} was assumed globally based on observations of the soil surface in tiger-bush in southwest Niger (Wallace and Holwill, 1997), but it was corrected (r_{corr}) for atmospheric temperature (T_i) and pressure (P_a) (Jones, 1992) with standard conditions assumed to be $T_i = 20°C$ and $P_a = 101300Pa$.

$$r_{corr} = \frac{1.0}{\frac{101300}{P_a} \times \left(\frac{T_i + 273.15}{293.15}\right)^{1.75}}$$

$$r_{tot} = r_{totc} \times r_{corr} \quad (31)$$

$r_{totc} = 107.0$

We assume that r_v (s m^{-1}) is equal to the aerodynamic resistance (r_a: s m^{-1}) in Equation 6 since the values of r_v and r_a are usually very close (van de Griend, 1994). The aerodynamic resistance at the soil surface (r_{as}) is parallel to both the resistance to convective heat transfer (r_{hs}: s m^{-1}) and the resistance to radiative heat transfer (r_{rs}: s m^{-1}) (Choudhury and DiGirolamo, 1998), such that

$$r_{as} = \frac{r_{hs} \times r_{rs}}{r_{hs} + r_{rs}}$$

$$r_{rs} = \frac{\rho \times C_p}{4.0 \times \sigma \times (T_i + 273.15)^3} \quad (32)$$

$r_{hs} = r_{tot}$

In the 2007 algorithm, only the soil evaporation from the moist surface was calculated. To examine the sensitivity of actual soil evaporation to r_{tot} in the 2007 MOD16 ET algorithm, we used different values for r_{totc}. The observed latent heat flux (LE) average over the 19 AmeriFlux towers used to validate the 2007 MOD16 algorithm was 66.9 W/m^2, while the average LE estimate was

61.0 W/m^2 driven by tower meteorological data and 65.6 W/m^2 driven by NASA's Global Modeling and Assimilation Office (GMAO, v. 4.0.0) data. When r_{totc} is 10 s m^{-1}, much lower than 107 s m^{-1}, soil evaporation is much higher, and hence LE is much higher, with the average tower-driven LE of 86.0 W/m^2 and GMAO-driven LE of 98.7 W/m^2. However, when r_{totc} ranges between 50 s m^{-1} and 1000 s m^{-1}, there is little difference in the soil evaporation results, and there is, therefore, little change in LE (tower-driven LE average of 54.4~64.6 W/m^2 and GMAO-driven LE average of 58.9~70.0 W/m^2). The value of 50 s m^{-1} was chosen in the 2007 algorithm as the lower bound because it is very close to the mean boundary layer resistance for vegetation under semiarid conditions, and there is little variation around this mean (van de Griend, 1994). In the improved MOD16 ET algorithm, the r_{hs} is assumed to be equal to boundary layer resistance, which is calculated in the same way as total aerodynamic resistance (r_{tot}) in Equation 31 (Thornton, 1998) only that, in the improved algorithm, r_{totc} is not a constant. For a given biome type, there is a maximum (rbl_{max}) and a minimum value (rbl_{min}) for r_{totc}, and r_{totc} is a function of VPD.

$$r_{totc} = \begin{cases} rbl_{max} & VPD \le VPD_{open} \\ rbl_{max} - \dfrac{(rbl_{max} - rbl_{min}) \times (VPD_{close} - VPD)}{VPD_{close} - VPD_{open}} & VPD_{open} < VPD < VPD_{close} \\ rbl_{min} & VPD \ge VPD_{close} \end{cases} \quad (33)$$

The values of rbl_{max} and rbl_{min}, VPD_{open} (when there is no water stress on transpiration) and VPD_{close} (when water stress causes stomata to close almost completely, halting plant transpiration) are parameterized differently for different biomes and are listed in Table 1.

The actual soil evaporation (λE_{SOIL}) is calculated in equation 34 using potential soil evaporation (λE_{SOIL_POT}) and soil moisture constraint function in the Fisher et al. (2008) ET model. This function is based on the complementary hypothesis (Bouchet, 1963), which defines land-atmosphere interactions from air *VPD* and relative humidity (*RH*, %).

$$\lambda E_{wet\_SOIL} = \frac{\left(s \times A_{SOIL} + \rho \times C_p \times (1.0 - F_C) \times VPD/r_{as}\right) \times Fwet}{s + \gamma \times r_{tot}/r_{as}}$$

$$\lambda E_{SOIL_{POT}} = \frac{\left(s \times A_{SOIL} + \rho \times C_p \times (1.0 - F_C) \times VPD/r_{as}\right) \times (1.0 - Fwet)}{s + \gamma \times r_{tot}/r_{as}} \quad (34)$$

$$\lambda E_{SOIL} = \lambda E_{wet\_SOIL} + \lambda E_{SOIL_{POT}} \times \left(\frac{RH}{100}\right)^{VPD/\beta}$$

where β was set as 100 in the 2007 algorithm, and is revised as 200 in the improved algorithm.

3.8 Total Daily Evapotranspiration

In the improved algorithm, the total daily ET is the sum of evaporation from the wet canopy surface, the transpiration from the dry canopy surface and the evaporation from the soil surface. The total daily ET and potential ET(λE_{POT}) are calculated as in equation 35.

$$\lambda E = \lambda E_{wet\_C} + \lambda E_{trans} + \lambda E_{SOIL} \quad (35)$$

$$\lambda E_{POT} = \lambda E_{wet\_C} + \lambda E_{POT\_trans} + \lambda E_{wet\_SOIL} + \lambda E_{SOIL_{POT}}$$

Combination of ET with the potential ET can determine environmental water stress and detect the intensity of drought.

4. Input Datasets

The MOD16 uses daily meteorological data and 8-day MODIS datasets as input for daily ET calculations. The input global daily meteorological dataset is from MERRA GMAO at about 0.5° × 0.6° resolution (http://disc.sci.gsfc.nasa.gov/daac-bin/FTPSubset.pl). For the MOD16 ET data product, the input MODIS datasets include 1) global 1-km^2 Collection 4 MODIS land cover type 2 (MOD12Q1) (Friedl et al., 2002), 2) global 1-km^2 MODIS Collection 5 FPAR/LAI (MOD15A2) (Myneni et al., 2002), and 3) Collection 5 global 1-km^2 albedo quality control and albedo data (the 10th band of the White-Sky-Albedo from MCD43B2/MCD43B3) (Schaaf et al., 2002; Jin et al., 2003; Salomon et al., 2006). Different from users' expectation, the Collection 5 MODIS FPAR/LAI is being generated with a frozen version of the Colleciton 4 instead of the Colleciton 5 MOD12Q1 land cover as an input by MODIS Adaptive Processing System (MODAPS) at NASA.

Table 3 Input non-satellite meteorological data, satellite data, and output ET data.

Variable Names	Sensors	Time Spans	Resolution		Coverage	Output Format
			Spatial	Temporal		
Input Non-Satellite Data (daily meteorological data)						
GMAO		2000-2006	1.00°x1.25°	daily	global	
MERRA GMAO		2000-present	0.5°x0.6°	daily	global	
Input Remote Sensing Data						
Albedo	MODIS (MOD43C)	2000-2006	0.05°	16-day	global	HDFEOS/ GEOTIFF
	MODIS (MCD43B)	2000-present	1km	8-day		
	VIIRS	2012-->				
Land Cover	MODIS		1km		global	HDFEOS/ GEOTIFF
	VIIRS					
LAI	MODIS	2000-present	1km		global	HDFEOS/ GEOTIFF
	VIIRS	2012-->				
FPAR	MODIS	2000-present	1km		global	HDFEOS/ GEOTIFF
	VIIRS	2012-->				
Output MOD16 ET products						
ET, LE, PET, PLE, QC	MODIS	2000-present	1km	8-day, monthly, annual	global	HDFEOS
	VIIRS	2012-->				

Table 3 lists the input and output datasets of the MOD16 ET algorithm. In Mu et al.'s 2011 MOD16 ET algorithm improvement paper, we used the GMAO (v4.0.0) global meteorological data at 1.00° × 1.25° resolution and Collection 4 0.05-degree CMG MODIS albedo (the 10th band of the White-Sky-Albedo from MOD43C1) to do the parameter calibrations and algorithm

validations over Jan. 2000-Dec. 2006. In this ATBD, we have two sets of Biome Properties Look-Up Table (BPLUT) as shown in Table 1.

4.1. Daily Meteorological Data

The MOD16 algorithm computes ET at a daily time step. This is made possible by the daily meteorological data, including average and minimum air temperature, incident PAR and specific humidity, provided by NASA's Global Modeling and Assimilation Office (GMAO or MERRA GMAO), a branch of NASA (Schubert et al. 1993). These data, produced every six hours, are derived using a global circulation model (GCM), which incorporates both ground and satellite-based observations. These data are distributed at a resolution of 0.5° x 0.6° (MERRA GMAO) or 1.00° x 1.25° (GMAO, v4.0.0) in contrast to the 1-km gridded MOD16 outputs. It is assumed that the coarse resolution meteorological data provide an accurate depiction of ground conditions and are homogeneous within the spatial extent of each cell.

Spatially interpolating GMAO reanalysis data

The resolution for GMAO (1.00° × 1.25°) or MERRA GMAO (0.5° x 0.6°) meteorological data is too coarse for a 1-km^2 MODIS pixel. Zhao et al. (2005) found that, in the Collection 4 MODIS GPP/NPP algorithm (MOD17), each 1-km^2 pixel falling into the same 1.00° × 1.25° GMAO grid cell inherited the same meteorological data, creating a noticeable GMAO footprint (Fig. 1a,c in Zhao et al., 2005). Such treatment may be acceptable on a global or regional scale, but it can lead to large inaccuracies at the local scale, especially for terrain with topographical variation or located in regions with steep climatic gradients. To enhance the meteorological inputs, Zhao et al. (2005) have non-linearly interpolated the coarse resolution GMAO data to the 1-km^2 MODIS pixel level based on the four GMAO cells surrounding a given pixel. Theoretically, this GMAO spatial interpolation improves the accuracy of meteorological data for each 1-km^2 pixel because it removes the abrupt changes from one side of a GMAO boundary to the other. In addition, for most World Meteorological Organization (WMO) stations, spatial interpolation reduced the root mean square error (RMSE) and increased the correlation between the GMAO data and the observed WMO daily weather data for 2000–2003, suggesting that the non-linear spatial interpolation considerably improves GMAO inputs. These interpolated GMAO data are, therefore, used in our calculations of ET.

4.2. Dependence on MODIS Land Cover Classification (MOD12Q1)

One of the first MODIS products used in the MOD16 algorithm is the Land Cover Product, MOD12Q1. The importance of this product cannot be overstated as the MOD16 algorithm relies heavily on land cover type through use of the BPLUT (Table 1). While, the primary product created by MOD12 is a 17-class IGBP (International Geosphere-Biosphere Programme) landcover classification map (Belward et al. 1999; Scepan 1999), the MOD16 algorithm employs University of Maryland (UMD) landcover classification scheme (Table 4). More details on these and other schemes and their quality control considerations can be found at the Land Cover Product Team website (*http://geography.bu.edu/landcover/userguidelc/index.html*). Given the global nature and daily

time-step of the MODIS project, a broad classification scheme, which retains the essence of land cover, is necessary. Since all MODIS products are designed at a 1-km^2 grid scale, it can be difficult to obtain accurate land cover in areas with complex vegetation, and misclassification can occur. However, studies have suggested that the MODIS vegetation maps are accurate to within 65-80%, with higher accuracies for pixels that are largely homogeneous, and allow for consistent monitoring of the global land cover (Hansen et al. 2000).

Table 4 The University of Maryland (UMD) landcover classification from MODIS land cover dataset (MOD12Q1) used in the MOD16 Algorithm. The data field name is Land_Cover_Type_2 in the MOD12Q1 data field.

UMD Land Cover Types	
Class Value	**Class Description**
0	Water
1	Evergreen Needleleaf Forest
2	Evergreen Broadleaf Forest
3	Deciduous Needleleaf Forest
4	Deciduous Broadleaf Forest
5	Mixed Forest
6	Closed Shrubland
7	Open Shrubland
8	Woody Savanna
9	Savanna
10	Grassland
12	Cropland
13	Urban or Built-Up
16	Barren or Sparsely Vegetated
254	Unclassified
255	Missing Data

4.3. Time Variable MODIS Input Data

As illustrated in Figure 2, the ET calculation also requires vegetation dynamic datasets, 8-day MODIS FPAR/LAI (MOD15), and surface albedo from 8-day MCD43B2/MCD43B3.

Fraction of absorbed photosynthetically active radiation (FPAR) and Leaf area index (LAI)

The FPAR/LAI product is an 8-day composite product. The MOD15 compositing algorithm uses a simple selection rule whereby the maximum FPAR (across the eight days) is chosen for the inclusion as the output pixel. The same day chosen to represent the FPAR measure also contributes the current pixel's LAI value. This means that although ET is calculated daily, the MOD16 algorithm necessarily assumes that leaf area and FPAR do not vary during a given 8-day period. Compositing of LAI and FPAR is required to provide an accurate depiction of global leaf area dynamics with consideration of spectral cloud contamination, particularly in the tropics.

MODIS Albedo

The MCD43B2/B3 albedo products are 8-day composite products. Both Terra and Aqua data are used in the generation of this product, providing the highest probability for quality input data and designating it as an "MCD," meaning "Combined," product. Version-5 MODIS/Terra+Aqua BRDF/Albedo products are Validated Stage 1, indicating that accuracy has been estimated using a small number of independent measurements obtained from selected locations and time periods and ground-truth/field program efforts. Although there may be later improved versions, these data are ready for use in scientific publications.

BRDF/Albedo Quality product (MCD43B2) describes the overall condition of the other BRDF and Albedo products. The MCD43B2 product contains 16 days of data at 1-km spatial resolution provided as a level-3 gridded data set in Sinusoidal projection, and includes albedo quality, snow conditions, ancillary information, and inversion information.

MCD43B3 product provides 1-km data describing both directional hemispherical reflectance (black-sky albedo) at local solar noon and bihemispherical reflectance (white-sky albedo). These MCD43B3 albedo quantities are produced from the16-day anisotropy models provided in MCD43B1 and represent averages of the underlying 500m values. If black-sky albedos at different solar zenith angles are required then the MCD43B1 values should be used directly to generate them. The MCD43B3 albedo quantities are provided as a level-3 gridded product in the Sinusoidal projection.

Temporally interpolating MODIS data with bad QC or missing data

The 8-day MOD15A2 LAI/FPAR (Myneni et al., 2002) and MCD43B3 (Schaaf et al., 2002; Jin et al., 2003; Salomon et al., 2006) contain some cloud-contaminated or missing data. We temporally filled the missing or unreliable LAI/FPAR and MCD43B3 albedo at each 1-km^2 MODIS pixel based on their corresponding quality assessment data fields as proposed by Zhao et al. (2005). The process entails two steps (see Fig. 5 in Zhao et al., 2005). If the first (or last) 8-day LAI/FPAR or MCD43B3 albedo is unreliable or missing, it will be replaced by the closest reliable 8-day value. This step ensures that the second step can be performed in which other unreliable LAI/FPAR or MCD43B3 albedo will be replaced by linear interpolation of the nearest reliable values prior to and after the missing data point.

Tropical rainforests, such as Amazon basin in South America, are the area where the cloud contamination is the most serious and the LAI seasonality is very small. To explore how the QC-controlled interpolations alter and enhance the input MODIS data quality, we compare the 8-day composited LAI in the Amazon for the original data integrated from MOD15A2 without the temporal interpolation and the enhanced LAI values with the interpolation for the period of March 21–28, 2001 during the wet season with the worst cloud contamination (Fig. 3). The original LAI values are too small (<2.0 m^2/m^2) for a large area surrounding the Amazon River, the result of severe cloud contamination. The MODIS land cover indicates most forests in the northern South America in Figure 3 are evergreen broadleaf forests (EBF). Field LAI observations revealed a mean LAI of 4.8±1.7 for 61 observations in tropical EBF (Asner et al.,

2003; Malhi et al., 2004, 2006). There are a few pixels for which the enhanced LAI values are smaller than the original data because of the bad QCs. Overall, however, after temporal filling, LAI values in Amazon are much higher and the spatial pattern is more realistic.

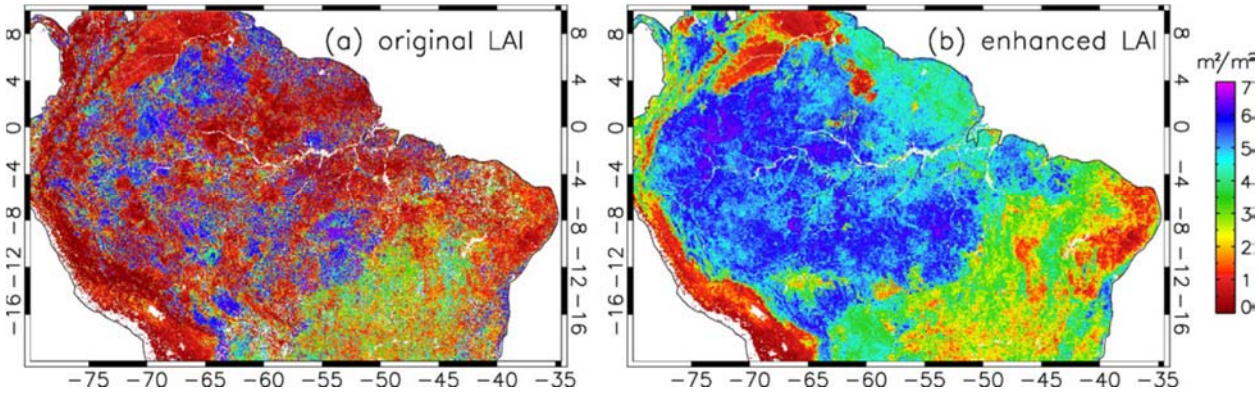

Figure 3 The 8-day composite leaf area index (LAI) in Amazon region for the 8-day period 081 (March 21–28) in 2001 for (a) the original with no temporal interpolation of the LAI and (b) the temporally interpolated LAI.

5. Parameterization of MOD16 ET Algorithm

Our method to calibrating parameters of BPLUT is largely based on the concept of water use efficiency (WUE), defined as the ratio of GPP to ET. WUEs derived from eddy flux towers are used together with the mature MODIS GPP dataset to estimate the expected mean annual ET for each biome. Below we first describe how we process measurements from flux towers, then we detail how we calibrate the BPLUT.

5.1. Eddy Covariance Flux Towers

The eddy covariance technique is a widely used and accepted method to measure ecosystem-scale mass and energy fluxes. The AmeriFlux network was established in 1996, providing continuous measurements of ecosystem level exchanges of CO_2, water, energy and momentum spanning diurnal, synoptic, seasonal, and interannual time scales and is currently composed of sites from North America, Central America, and South America (http://public.ornl.gov/ameriflux/). AmeriFlux is part of a "network of regional networks" (FLUXNET) including more than 500 tower sites from about 30 regional networks across five continents, providing half-hourly to hourly measurements of carbon dioxide, water vapor, and energy exchanges between terrestrial ecosystems and the atmosphere across a diverse range of ecosystems and climates on a long-term basis (Baldocchi, 2008; http://www.daac.ornl.gov/FLUXNET/fluxnet.html). The insights and constraints provided by the simultaneous measurement of these fluxes and their corresponding scalar fields ensure that Fluxnet provides an excellent data set for land surface model development and testing.

We obtained the level 4 measured meteorological data and latent heat flux (LE) data at 72 AmeriFlux eddy covariance towers to calibrate parameters and test the performance of MOD16 ET algorithm. To ensure a reliable measured data from these towers, first, 51 towers were left after we excluded those towers with actual vegetation type different from MOD12 land cover type 2 at any of the surrounding 3 x 3 1-km^2 pixels. Then we further excluded those towers with fewer than half a year of measurements during 2000-2006. As a result, there are 46 AmeriFlux eddy covariance tower sites involved in WUE calaulation and evaluation of the algorithm. The tower measured ET in water depth was calculated from tower measured LE data using the following equation,

$$ET = \frac{LE}{\lambda} \qquad (36)$$

where λ is the latent heat of vaporization (J kg^{-1}). MOD16 ET algorithm was tested at these 46 AmeriFlux eddy covariance tower sites (Table 5, Fig. 4) with available level 4 ET measurements over 2000-2006. These 46 flux towers cover nine typical land cover types and a wide range of climates. The nine land cover types among the towers include evergreen needleleaf forest (ENF), evergreen broadleaf forest (EBF), deciduous broadleaf forest (DBF), mixed forest (MF), open shrublands (OSH), close shrublands (CSH), woody_savanas (WL), grasslands (Grass), and croplands (Crop).

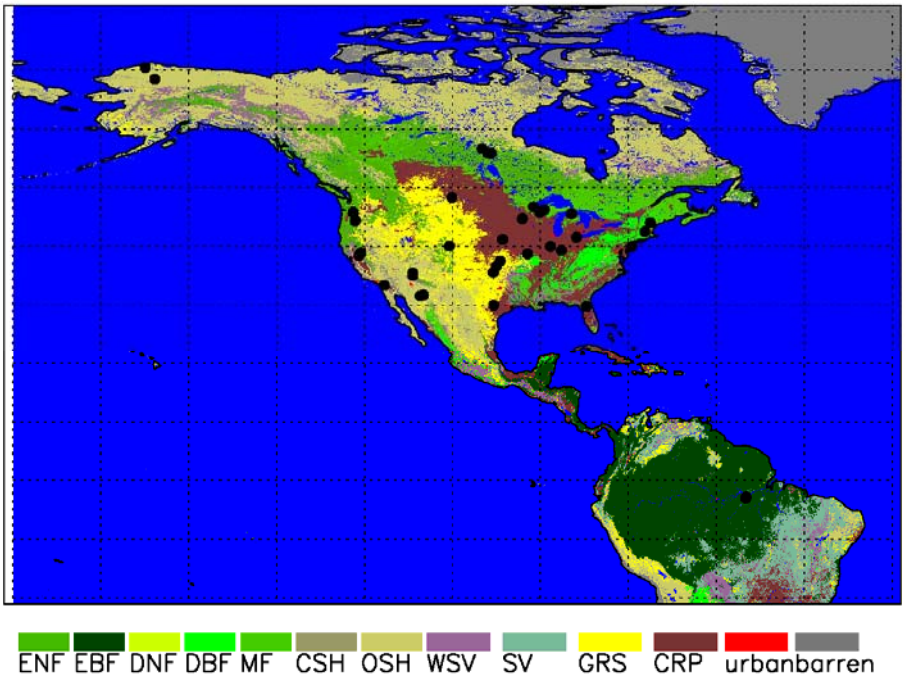

Figure 4 Distribution of the 46 AmeriFlux eddy flux towers used for validation of the improved ET algorithm. The background is the MOD12Q1 land cover type 2, with the blue color for the water body.

Table 5 The tower names, abbreviations, latitude (lat), longitude (lon), biome types in the parentheses, number of days with valid tower measurements (Days), average daily tower evapotranspiration measurements over all the days with valid values (ET_OBS: mm/day).

Site	Abbrev.	lat	lon	Days	ET_OBS
ARM_SGP_Main	**USARM (Crop)**	36.6	-97.5	1129	1.43
Bondville	**USBo1 (Crop)**	40.0	-88.3	1616	1.82
Mead_Irrigated	**USNe1 (Crop)**	41.2	-96.5	1080	1.62
Mead_Irrigated_Rotation	**USNe2 (Crop)**	41.2	-96.5	1022	1.56
Mead_Rainfed	**USNe3 (Crop)**	41.2	-96.4	1027	1.46
Rosemount_G19_Alternative_Management_Corn_Soybean_Rotation	**USRo3 (Crop)**	44.7	-93.1	573	1.35
Rosemount_G21_Conventional_Management_Corn_Soybean_Rotation	**USRo1 (Crop)**	44.7	-93.1	574	1.39
Sky_Oaks_Old	**USSO2 (CSH)**	33.4	-116.6	333	1.04
Bartlett_Experimental_Forest	**USBar (DBF)**	44.1	-71.3	614	0.84
Missouri_Ozark	**USMOz (DBF)**	38.7	-92.2	606	2.20
Morgan_Monroe_State_Forest	**USMMS (DBF)**	39.3	-86.4	1483	1.16
Ohio_Oak_Openings	**USOho (DBF)**	41.6	-83.8	371	1.94
UMBS	**USUMB (DBF)**	45.6	-84.7	1205	1.22
Willow_Creek	**USWCr (DBF)**	45.8	-90.1	1246	0.97
LBA_Tapajos_KM67_Mature_Forest	**BRSa1 (EBF)**	-2.9	-55.0	1008	3.08
LBA_Tapajos_KM83_Logged_Forest	**BRSa3 (EBF)**	-3.0	-55.0	1281	3.63
Blodgett_Forest	**USBlo (ENF)**	38.9	-120.6	1586	1.99
Donaldson	**USSP3 (ENF)**	29.8	-82.2	1585	2.68
Flagstaff_Unmanaged_Forest	**USFuf (ENF)**	35.1	-111.8	308	1.24
Metolius_First_Young_Pine	**USMe5 (ENF)**	44.4	-121.6	545	0.99
Metolius_Intermediate_Pine	**USMe2 (ENF)**	44.5	-121.6	707	1.18
Metolius_New_Young_Pine	**USMe3 (ENF)**	44.3	-121.6	361	0.93
Niwot_Ridge	**USNR1 (ENF)**	40.0	-105.5	1535	1.54
UCI_1850	**CANS1 (ENF)**	55.9	-98.5	429	0.56
UCI_1930	**CANS2 (ENF)**	55.9	-98.5	431	0.57
UCI_1964	**CANS3 (ENF)**	55.9	-98.4	488	0.54
UCI_1964wet	**CANS4 (ENF)**	55.9	-98.4	236	0.38
UCI_1981	**CANS5 (ENF)**	55.9	-98.5	503	0.58
UCI_1989	**CANS6 (ENF)**	55.9	-99.0	494	0.53
UCI_1998	**CANS7 (ENF)**	56.6	-99.9	411	0.59
Wind_River_Crane_Site	**USWrc (ENF)**	45.8	-122.0	974	1.54
Wisconsin_Mature_Red_Pine	**USWi4 (ENF)**	46.7	-91.2	308	2.09
ARM_SGP_Burn	**USARb (Grass)**	35.5	-98.0	553	2.15
ARM_SGP_Control	**USARc (Grass)**	35.5	-98.0	554	2.36
Atqasuk	**USAtq (Grass)**	70.5	-157.4	244	0.11

Audubon_Grasslands	**USAud (Grass)**	31.6	-110.5	1431	0.78
Kendall_Grassland	**USWkg (Grass)**	31.7	-109.9	929	0.63
Walnut_River	**USWlr (Grass)**	37.5	-96.9	885	1.86
Fort_Peck	**USFPe (Grass)**	48.3	-105.1	1095	0.77
Fort_Dix	**USDix (MF)**	40.0	-74.4	412	1.56
Little_Prospect_Hill	**USLPH (MF)**	42.5	-72.2	667	1.35
Sylvania_Wilderness	**USSyv (MF)**	46.2	-89.3	825	0.89
Ivotuk	**USIvo (OSH)**	68.5	-155.8	210	0.19
Flagstaff_Wildfire	**USFwf (WL)**	35.4	-111.8	338	0.94
Freeman_Ranch_Mesquite_Juniper	**USFR2 (WL)**	29.9	-98.0	649	2.08
Tonzi_Ranch	**USTon (WL)**	38.4	-121.0	1342	1.13
Average					**1.34**

5.2 Pre-processing Tower Observed Data

The AmeriFlux tower data are given every 30 minutes. When the number (*N*) of the reliable 30-minute measurements is no less than 40 a day, the daily average values of the incoming solar radiation (*SWrad*), air temperature (*Tavg*), *VPD*, and *LE* are the averages of these measurements. For each 30-minute time period, ET (mm/30minutes) is calculated as

$$\lambda = (2.501 - 0.002361 \times T_n) \times 10^6$$

$$ET_n = \frac{LE_n \times 60.0 \times 30.0}{\lambda} \qquad (37)$$

where n is the nth 30-minute observation of each day, λ is calculated using the equation in Maidment's book (Maidment, 1993). When the number of the reliable 30-minute measurements (*N*) of both *LE* and T are no less than 40, the daily total ET is calculated as

$$ET = \frac{\sum_{n=1}^{N} ET_n \times 48}{N} \qquad (38)$$

If *N* is less than 40, the daily measurements are set as fill value. The daily maximum and minimum air temperatures are obtained through the process when calculating the daily average air temperature.

The daytime and nighttime are distinguished by *SWrad*. If *SWrad >10.0* (W m^{-2}), it's daytime, otherwise, nighttime. The measured daytime *VPD* (*VPDday*) and air temperature (*Tday*), and nighttime *VPD* (*VPDnight*) and air temperature (*Tnight*) are the averages over daytime and nighttime. When there are fewer than 20 reliable measurements during daytime or nighttime, both daytime and nighttime values are set as fill value.

5.3 Parameterization

For parameterization of the improved ET algorithm, we largely follow the method for calibrating parameters of MODIS GPP/NPP algorithm (Zhao et al., 2005). Both MODIS GPP/NPP and MODIS ET algorithms use the same controlling factors from *VPD* and minimum temperature (*Tmin*) on stomatal conductance. We first adopt the parameters of *VPD* and *Tmin* setting from those for MODIS GPP/NPP algorithm (Table 1), then calibrate other parameters for each biome. Below we detail the procedure to parameterize MODIS ET.

The tower derived annual GPP and tower measured annual ET were summed over all the available days divided by the number of years (≤365 days/yr). Then annual average WUE for each tower site was calculated as

$$WUE = \frac{GPP}{ET} \qquad (39)$$

For a given biome type in Table 1, the tower GPP, ET and WUE are averaged over all the towers with the same biome (Table 6). Finally, the expected annual total ET for a given biome is calculated by using the multiyear mean annual total MODIS GPP (Zhao et al., 2005) and tower-based WUE (listed in Table 6) as

$$ET_{exp} = \frac{MODIS\ GPP}{WUE} \qquad (40)$$

We use ET_{exp} as one target (Table 6) to calibrate other parameters in Biome-Property-Look-Up-Table (BPLUT) except T_{min} and *VPD*, which are directly adopted from MODIS GPP parameters as mentioned above. Each time, the improved ET algorithm is run globally using a set of parameter values at the 0.5° resolution over 2000-2006. The annual MODIS GPP and estimated annual MODIS ET averaged globally for each biome type (ET_{mod}) may greatly differ from the tower GPP and ET_{exp} because, 1) only 46 AmeriFlux tower sites are used to get tower GPP, ET and WUE, and thus they may not represent average conditions for a biome type at the global scale; 2) WUE is the water use efficiency, which should be the ratio of GPP to ET via transpiration. Considering the evaporation included in ET, there is some bias in the calculated WUE and hence ET_{exp} (Law et al., 2002). Therefore, when we calibrate parameters in BPLUT at global scale, not only ET_{mod} is compared to ET_{exp}, but also the spatial pattern of average annual ET over 2000-2006 is compared with Chen et al.'s 0.5° global precipitation data (Chen et al, 2002). At the arid and semi-arid areas, up to 50% or even higher than 100% of the annual precipitation is returned to the atmosphere as ET (Mellouli et al.; 2000). At the local scale, the improved ET algorithm is run at the 46 tower sites and the RMSE between the daily ET estimates and ET measurements is calculated. We modify BPLUT and repeat the cycle of comparison till we choose one set of parameter values that perform the best both globally and locally for BPLUT (Table 1). There are no towers with deciduous needle-leaf forest (DNF) or savannas (SV) in the 46 AmeriFlux towers.

We made an assumption that the ET for the DNF should be close to the one for ENF, and the ET for SV should be a little lower than the one for woody savannas.

Table 6 The tower measured annual GPP, tower measured annual ET summed over all the available days divided by the number of years (≤365 days/year), and WUE calculated from equation (39) averaged over all the towers for each vegetation type; the annual MODIS GPP averaged over each vegetation type; the expected MODIS ET as calculated from equation (40); the actual average annual MODIS ET over each vegetation type. ENF: evergreen needleleaf forest; EBF: evergreen broadleaf forest; DNF: deciduous needleleaf forest; DBF: deciduous broadleaf forest; MF: mixed forest; WL: woody savannas; SV: savannas; CSH: closed shrubland; OSH: open shrubland; Grass: grassland, urban and built-up, barren or sparsely vegetated; Crop: cropland. N/A means that no data is available.

LC	Tower annual GPP (g C/m^2/yr)	Tower annual ET (mm/yr)	Annual WUE (g C/mm/m^2)	Annual MODIS GPP (g C/yr)	Expected annual MODIS ET (mm/yr)	Actual MODIS ET1* (mm/yr)	Actual MODIS ET2* (mm/yr)
ENF	978.98	423.64	2.42	876.78	362.89	301.01	304.63
EBF	2781.55	1123.03	2.51	2698.53	1073.96	1180.16	1182.63
DNF	N/A	N/A	N/A	727.00	N/A	334.57	349.54
DBF	1303.88	449.44	3.01	1340.12	444.94	533.47	474.53
MF	911.17	332.88	2.84	1133.64	398.60	488.12	499.44
CSH	909.51	484.82	1.80	811.91	451.88	333.31	334.66
OSH	193.60	160.2	1.35	308.79	229.04	272.34	270.19
WL	625.81	353.39	1.70	1368.58	805.20	925.62	944.41
SV	N/A	N/A	N/A	1209.21	N/A	749.52	792.09
Grass	645.68	417.06	1.46	393.09	269.71	352.65	350.39
Crop	1089.70	536.79	1.97	883.91	447.82	472.84	470.49

1* means the MODIS ET driven by v4.0.0 GMAO; 2* means MODIS ET driven by MERRA GMAO

6. Results and Uncertainties

In this section, we show the validation results of MOD16 ET at eddy flux towers, global 232 watersheds, as well as global results over the past 11 years (2000 to 2010). We also discuss the sources of uncertainties to the global MOD16 ET product.

6.1 Algorithm Performance at the Eddy Flux Tower Sites

We cut out the input MODIS data for the 3 x 3 1-km^2 pixels surrounding each tower. We drove the MOD16 ET algorithm with both tower observed meteorological data and global GMAO

meteorological data. We got the average ET estimates over those of the 3 x 3 1-km^2 pixels where the tower actual vegetation type is the same as MOD12 land cover type 2. Then we compared the ET estimates with the tower ET observations. For each of the seven biome types among the 46 flux towers except for CSH and OSH since there is only one tower with fewer than 365 measurements for each of them, we chose one tower to show the performance of MOD16 ET algorithm (Fig. 5). We use the Taylor skill score (Taylor, 2001) to evaluate the skill of the performances (Table 7).

$$S = \frac{4 \times (1 + R)}{(\hat{\sigma} + 1/\hat{\sigma})^2 \times (1 + R_0)} \qquad (41)$$

where R is the correlation coefficient, R_0 is theoretical maximum correlation, and $\hat{\sigma}$ is the standard deviation of ET estimates normalized by the standard deviation of ET measurements.

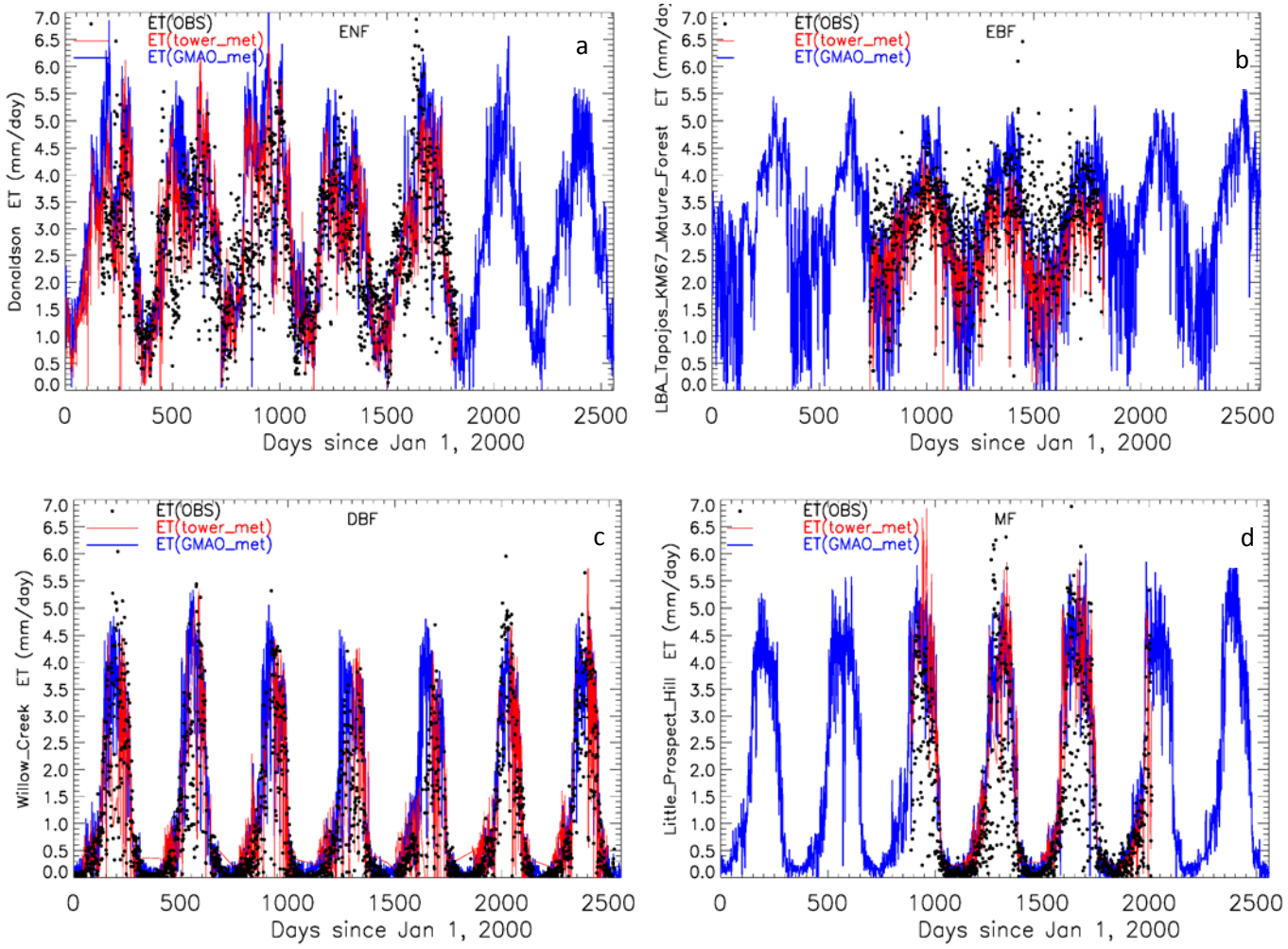

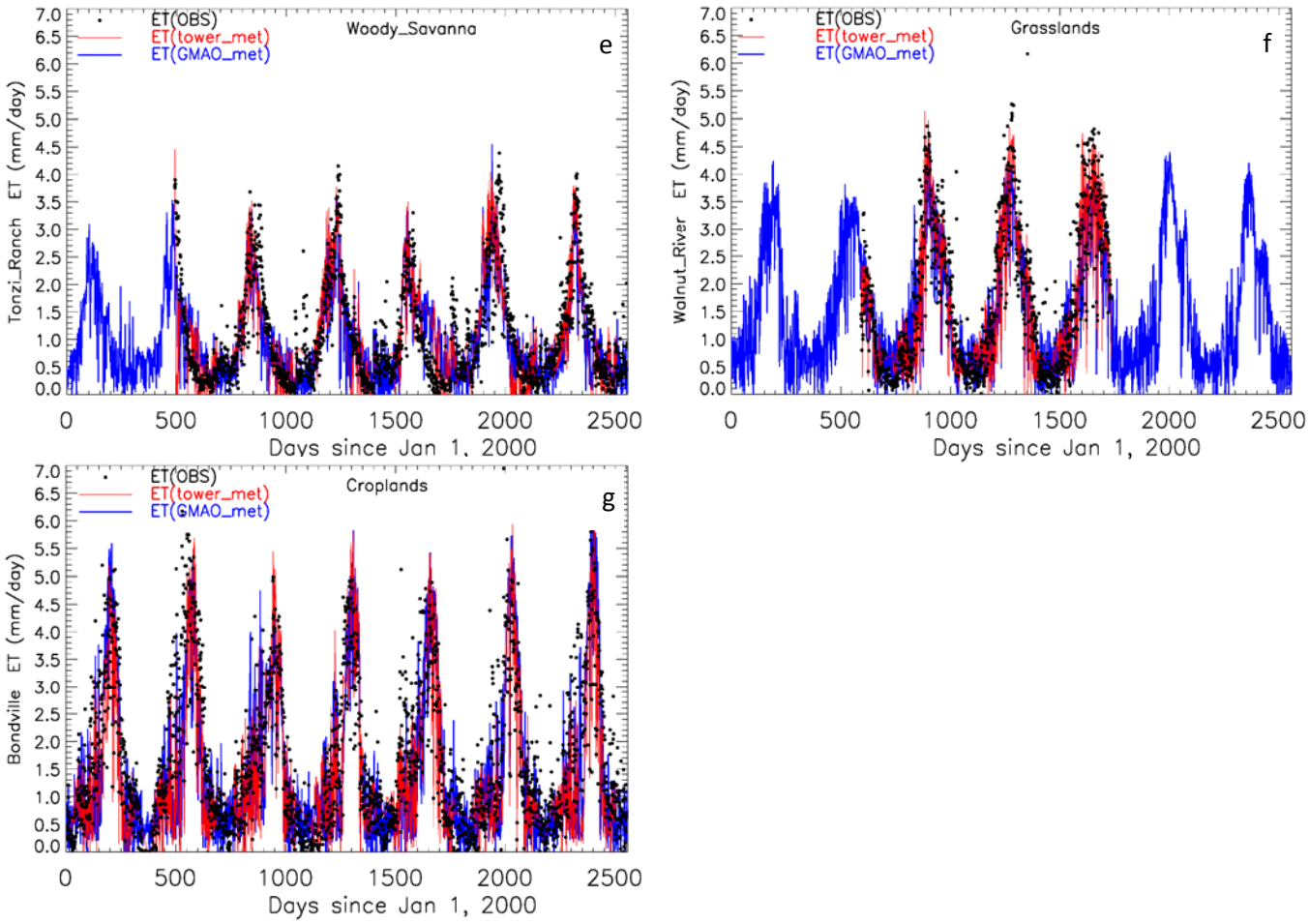

Figure 5 The ET measurements (black dots, OBS), the ET estimates driven by flux tower measured meteorological data (red lines) and GMAO meteorological data (blue lines) over 2000-2006 at seven tower sites, Donaldson (a), LBA Tapajos KM67 Mature Forest (b), Willow Creek (c), Little Prospect Hill (d), Tonzi Ranch (e), Walnut River (f) and Bondville (g).

The average daily ET biases between ET observations and ET estimates across the 46 towers are -0.11 mm/day driven by tower meteorological data and -0.02 mm/day driven by GMAO meteorological data (Table 7). The average mean absolute errors (MAE) are 0.33 mm day^{-1} (tower-specific meteorology) and 0.31 mm day^{-1} (GMAO meteorology). The MAE values are 24.6% and 24.1% of the ET measurements, within the 10-30% range of the accuracy of ET observations (Courault et al. 2005; Jiang et al. 2004; Kalma et al. 2008). The scores are 0.55 (tower-specific) and 0.53 (GMAO) across the 46 towers.

Table 7 The tower abbreviations, average daily tower evapotranspiration (ET) measurements over all the days with valid values (ET_OBS: mm/day); the biases (BIAS: mm/day), mean absolute biases (MAE: mm/day), correlation coefficients (R) and Taylor skill scores (S) of ET estimates relative to tower ET measurements for the 46 AmeriFlux eddy flux towers. 1: tower-driven results; 2: GMAO-driven results.

Site	ET_OBS	BIAS1	BIAS2	MAE1	MAE2	R1	R2	S1	S2	Citations
USARM (Crop)	1.43	-0.62	-0.3	0.62	0.3	0.42	0.41	0.76	0.71	
USBo1 (Crop)	1.82	-0.3	-0.16	0.3	0.16	0.78	0.73	0.54	0.61	
USNe1 (Crop)	1.62	-0.6	-0.48	0.6	0.48	0.87	0.81	0.45	0.70	
USNe2 (Crop)	1.56	-0.62	-0.48	0.62	0.48	0.85	0.80	0.12	0.05	
USNe3 (Crop)	1.46	-0.47	-0.35	0.47	0.35	0.85	0.79	0.31	0.45	
USRo3 (Crop)	1.35	-0.22	-0.21	0.22	0.21	0.72	0.75	0.38	0.50	
USRo1 (Crop)	1.39	-0.27	-0.26	0.27	0.26	0.71	0.72	0.32	0.23	
USSO2 (CSH)	1.04	-0.71	-0.51	0.71	0.51	0.02	0.06	0.86	0.82	
USBar (DBF)	0.84	0.48	0.66	0.48	0.66	0.90	0.83	0.68	0.58	Jenkins et al., 2007
USMOz (DBF)	2.2	-0.03	-0.08	0.03	0.08	0.84	0.76	0.10	0.16	
USMMS (DBF)	1.16	0.27	0.27	0.27	0.27	0.88	0.82	0.43	0.53	
USOho (DBF)	1.94	-0.14	-0.17	0.14	0.17	0.86	0.83	0.44	0.29	
USUMB (DBF)	1.22	-0.02	0.05	0.02	0.05	0.93	0.89	0.25	0.36	
USWCr (DBF)	0.97	0.18	0.35	0.18	0.35	0.91	0.85	0.77	0.89	Cook et al., 2004
BRSa1 (EBF)	3.08	-0.44	-0.11	0.44	0.11	0.76	0.33	0.64	0.17	Hutyra et al., 2007; Rocha et al., 2009; Fisher et al., 2009
BRSa3 (EBF)	3.63	-0.29	-0.45	0.29	0.45	0.62	0.35	0.65	0.73	
USBlo (ENF)	1.99	-0.57	-0.58	0.57	0.58	0.65	0.24	0.87	0.35	
USSP3 (ENF)	2.68	0.28	0.51	0.28	0.51	0.52	0.48	0.80	0.50	Gholz & Clark, 2002; Clark et al., 2004
USFuf (ENF)	1.24	-0.59	-0.61	0.59	0.61	0.62	0.42	0.66	0.72	
USMe5 (ENF)	0.99	-0.11	0.01	0.11	0.01	0.25	0.26	0.28	0.26	Anthoni et al., 2002
USMe2 (ENF)	1.18	-0.08	-0.1	0.08	0.1	0.32	0.29	0.25	0.24	Thomas et al., 2009
USMe3 (ENF)	0.93	-0.37	-0.12	0.37	0.12	0.39	0.38	0.41	0.40	Vickers et al., 2010
USNR1 (ENF)	1.54	-0.66	-0.69	0.66	0.69	0.68	0.64	0.60	0.59	
CANS1 (ENF)	0.56	0.1	0.04	0.1	0.04	0.74	0.70	0.56	0.52	
CANS2 (ENF)	0.57	0.08	0.03	0.08	0.03	0.78	0.75	0.14	0.26	
CANS3 (ENF)	0.54	0.12	0.11	0.12	0.11	0.75	0.73	0.77	0.85	
CANS4 (ENF)	0.38	0.24	0.27	0.24	0.27	0.71	0.76	0.85	0.87	
CANS5 (ENF)	0.58	0.18	0.19	0.18	0.19	0.77	0.71	0.46	0.48	
CANS6 (ENF)	0.53	0.14	0.09	0.14	0.09	0.76	0.72	0.92	0.92	
CANS7 (ENF)	0.59	-0.11	-0.17	0.11	0.17	0.74	0.69	0.67	0.72	
USWrc (ENF)	1.54	0.94	0.67	0.94	0.67	0.48	0.41	0.67	0.70	
USWi4 (ENF)	2.09	0.34	0.41	0.34	0.41	0.29	0.25	0.30	0.15	
USARb (Grass)	2.15	-0.51	-0.43	0.51	0.43	0.90	0.86	0.46	0.43	
USARc (Grass)	2.36	-0.77	-0.63	0.77	0.63	0.90	0.86	0.89	0.78	
USAtq (Grass)	0.11	0.02	0.16	0.02	0.16	0.11	-0.03	0.63	0.70	
USAud (Grass)	0.78	-0.37	-0.07	0.37	0.07	0.47	0.40	0.73	0.74	
USWkg (Grass)	0.77	-0.19	0	0.19	0	0.51	0.46	0.62	0.62	

USWlr (Grass)	0.63	-0.3	0.11	0.3	0.11	0.85	0.80	0.22	0.13	
USFPe (Grass)	1.86	-0.15	-0.2	0.15	0.2	0.27	0.26	0.62	0.56	
USDix (MF)	1.56	0.43	0.87	0.43	0.87	0.69	0.68	0.51	0.54	
USLPH (MF)	1.35	0.81	0.83	0.81	0.83	0.86	0.76	0.66	0.54	Hadley et al., 2008
USSyv (MF)	0.89	0.47	0.62	0.47	0.62	0.81	0.78	0.93	0.92	Desai et al., 2005
USIvo (OSH)	0.19	0.02	0.02	0.02	0.02	0.35	-0.01	0.92	0.86	
USFwf (WL)	0.94	-0.43	-0.31	0.43	0.31	0.24	0.35	0.86	0.87	
USFR2 (WL)	2.08	-0.1	0.29	0.1	0.29	0.69	0.79	0.10	0.31	
USTon (WL)	1.13	0.01	0.02	0.01	0.02	0.78	0.75	0.37	0.32	Baldocchi et al., 2004; Xu & Baldocchi 2003
Average	**1.34**	**-0.11**	**-0.02**	**0.33**	**0.31**	**0.65**	**0.58**	**0.55**	**0.53**	

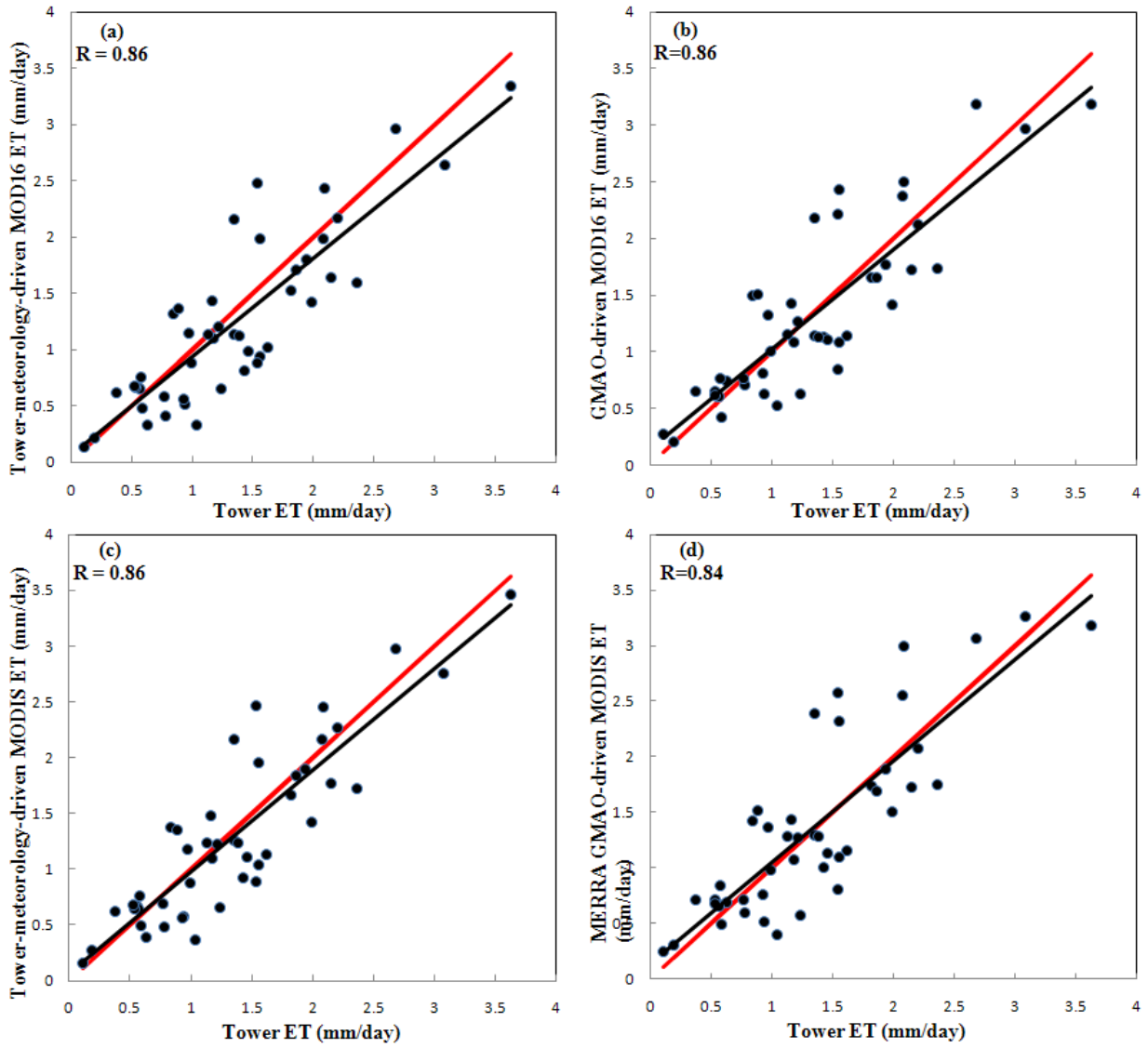

Figure 6 Comparisons of the average ET observations to the average daily ET estimates with the GMAO parameterized algorithm (a,b) and MERRA GMAO parameterized algorithm (c, d) across all the available

days at the 46 flux tower sites. These data were created using (1) tower-specific meteorology (a, c), (2) global GMAO meteorology (b) and MERRA GMAO meteorology (d). The solid red lines represent that the ratio of ET estimates to ET measurements is 1.0 and the solid black lines are the regression of the ET estimates to measurements.

Figure 6 shows the comparisons of the average ET observations to the average daily ET estimates across all the available days at the 46 flux tower sites. Both the GMAO parameterized algorithm and MERRA GMAO parameterized algorithm were driven by tower-specific meteorology (Fig. 6a, 6c) and the global meteorology (Fig. 6b, 6d). The correlation coefficients between MOD16 ET estimates and the ET observations are 0.86 (tower-specific, Fig. 6a, 6c), 0.86 (GMAO-driven, Fig. 6b) and 0.84 (MERRA GMAO-driven, Fig. 6d).

6.2 Implementing ET Algorithm at the Global Scale

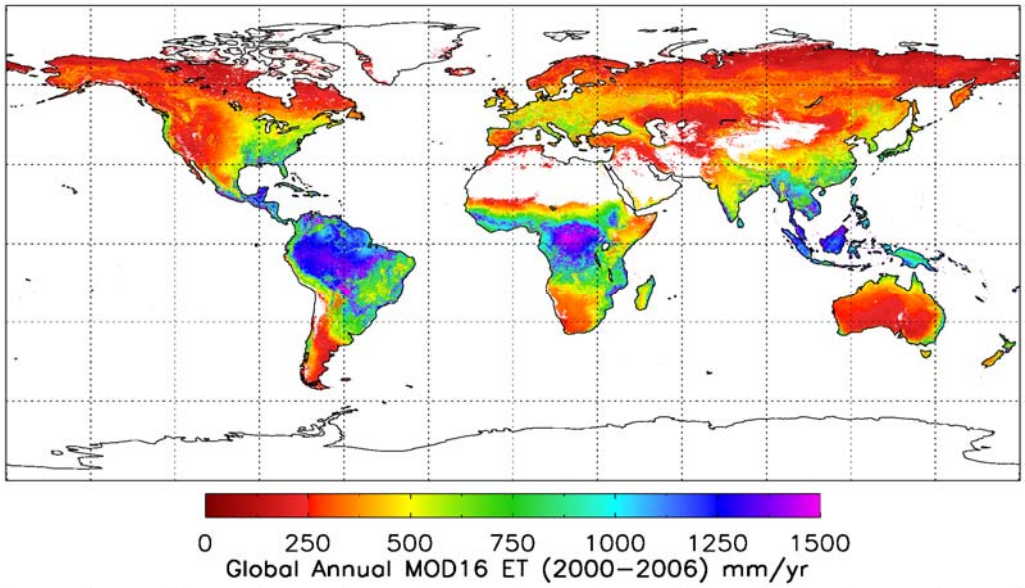

Figure 7 Global annual MOD16 evapotranspiration (top) over 2000-2006 driven by global GMAO (v4.0.0) meteorological data and (bottom) over 2000-2010 driven by global MERRA GMAO meteorological data.

MOD16 ET algorithm were implemented globally at 1-km^2 resolution using the preprocessed MODIS remote sensing data and 1) GMAO meteorological data over 2000-2006, 2) MERRA GMAO meteorological data over 2000-2010 as detailed in section 4. Figure 7 shows that the highest ET happens over the tropical forests, whereas dry areas and areas with short growing seasons have the lowest estimates of ET. The ET for temperate and boreal forests lies between the two extremes (Fig. 7). Averaged over 2000-2006 (GMAO-driven) and 2000-2010 (MERRA-GMAO driven), the total global annual ET over the vegetated land surface is 62.8×10^3 km^3, and 63.4×10^3 km^3, respectively, a little less than 65.5×10^3 km^3 reported by Oki and Kanae (2006), because MOD16 ET doesn't include urban and barren areas since there is no MODIS derived FPAR/LAI for these land cover types. Figure 8 shows the histograms of the global annual ET by both GMAO and MERRA GMAO meteorological datasets. The GMAO-driven global ET has a global average of 568 ± 378 mm yr^{-1}, and the MERRA GMAO-driven global ET has a global average of 569 ± 358 mm yr^{-1}.

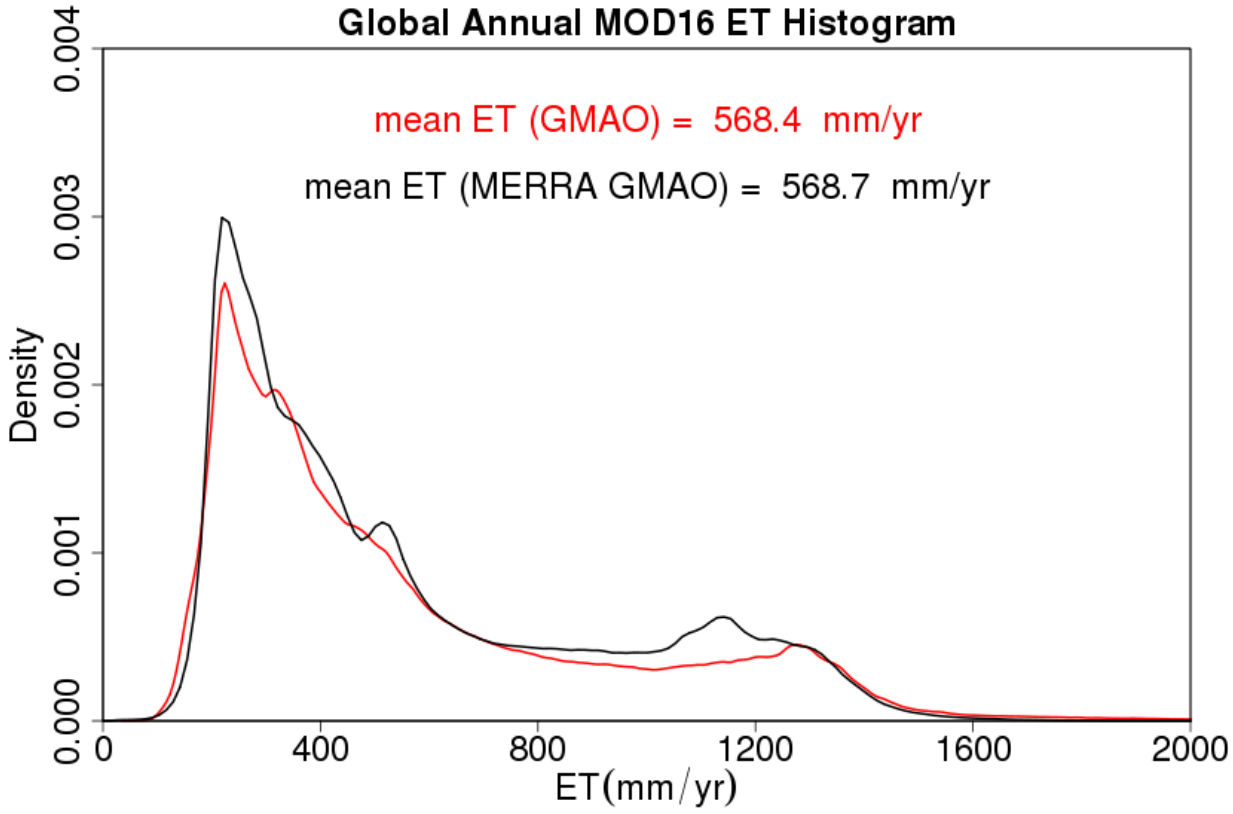

Figure 8 Comparison of the histograms of climatological average of global annual evapotranspiration driven by GMAO meteorological data (red solid line) over 2000-2006 and by MERRA GMAO meteorological data (solid black line) over 2000-2010. The GMAO-driven global average ET is 568.4 mm/yr and 568.7 mm/yr driven by MERRA GMAO meteorology (see text). These comparisons are only for vegetated land surfaces. The vegetated land area is shown as the colored area in Fig. 7.

Based on MOD12Q1 land cover types 2, barren/deserts take up 24% of the Earth's land surface. If we assume that the ET from the barren/deserts is zero, the average MODIS ET estimate with the improved algorithm over the entire land surface is 568*(100-24)/100=432 mm yr^{-1} (GMAO-driven) or 569*(100-24)/100=432 mm yr^{-1} (MERRA GMAO-driven). In reality, ET at the barren/deserts is not zero, so the ET estimates should be in the range of a little higher than 432 (432) mm yr^{-1}. Over the entire land surface of the globe, precipitation averages around 750 mm yr^{-1} (Fisher et al., 2005). Some studies concluded that ET returns more than 60% of precipitation on land back to the atmosphere (Korzoun et al., 1978; L'vovich and White, 1990). Based on these published data, the actual ET over the global land surface should be around 750*60%=450mm yr^{-1}. Our average MODIS ET estimate by the improved algorithm over the complete land surface is very close to the actual ET calculated from precipitation.

Figure 9 shows zonal mean of global annual ET driven by GMAO over 2000-2006. The peak happens at the southern tropical area, with the second peak at the northern tropical area where rainforests exist. Liski et al. (2003) reported that the ET in boreal and temperate forests across Europe (34 sites) ranged from 328 to 654 mm yr^{-1}, while the average ET was 466 mm yr^{-1} for Canada (18 sites) and 642 mm yr^{-1} for the US and Central America (26 sites) for biomes ranging from arctic tundra to tropical rainforest. MOD16 ET estimates in boreal and temperate forests are within the range of these reported ET from field data.

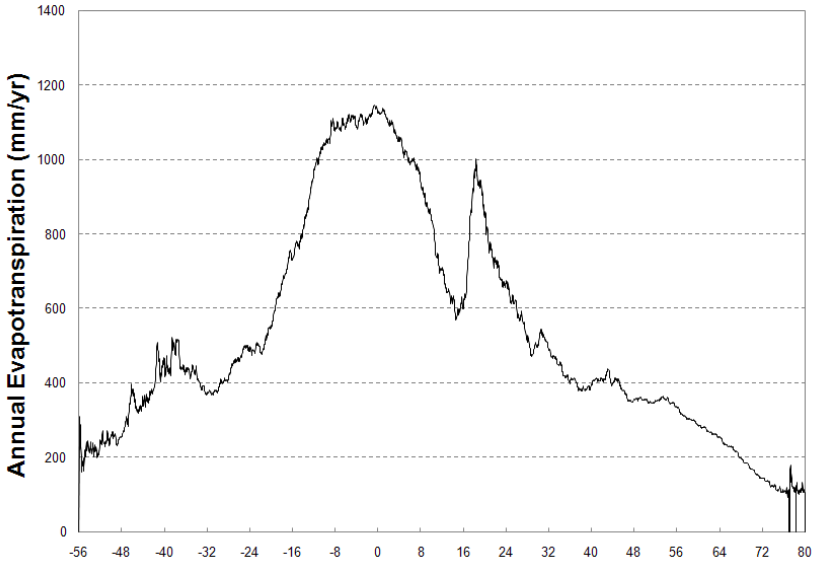

Figure 9 Climatological zonal mean of global annual evapotranspiration by GMAO meteorological data over 2000-2006.

Seasonality

Over 2000-2010, the ability of MOD16 ET algorithm to capture seasonality has been examined. Figure 10 shows the seasonality of global MOD16 ET. In the Northern Hemisphere, spring (MAM, Fig. 10) is the onset of the growing season. ET increases, reaching a peak in summer (JJA). In autumn (SON), ET begins to drop, with the lowest values in winter (DJF). Regionally, JJA and SON are relatively dry seasons in the Amazon, and Huete et al. (2006) found that vegetation grows better in dry seasons than in wet seasons (MAM and DJF). Transpiration, the

major component of ET in dense vegetation, dominates. Therefore, plants grow better during JJA and SON, and ET is higher (Fig. 10). Hutyra et al. (2007) also found that ET and GPP are higher at a rainforest flux tower in Amazon in dry seasons than in wet seasons.

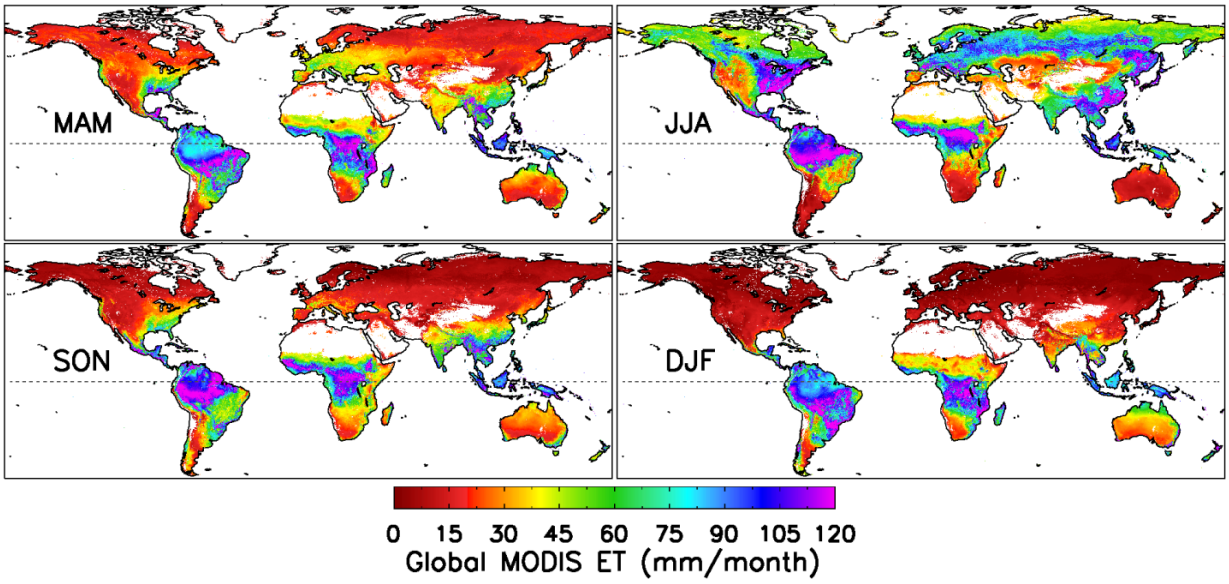

Figure 10 Spatial pattern of the global MOD16 ET seasonality during 2000-2010.

Interannual variability

The MOD16 ET algorithm also has the ability to capture the responses of terrestrial ecosystems to extreme climatic variability at the regional scale. We drove the MOD16 ET algorithm with global MERRA GMAO meteorological data and Collection 5 1-km^2 MCD43B2/MCD43B3 to produce the 1-km^2 global terrestrial MOD16 ET product over 2000-2010. The ratio of ET to PET is commonly used as an indicator of wetness or droughts. Figure 11 shows the anomalies of global ET to PET ratio at growing season from 2000-2009 as estimated from the MODIS-based ET product, demonstrating the sensitivity of terrestrial ecosystem to widespread drought in North America and China in 2000 (Cook et al., 2007; Fan et al., 2003; Pandey et al., 2007); extensive drought over North America and Australia in 2002 (Cook et al., 2007; Lawrimore et al., 2002; Horridge et al., 2005); heat wave in Europe (Ciais, et al., 2005) and drought in Australia in 2003 (Nicholls, 2004); severe droughts in Amazon, Africa and Australia in 2005 (Phillips et al., 2009; Hopkin, 2005; Watkins, 2005). However, a negative anomaly of ET/PET ratio in southern China in 2008 was not caused by drought but by damaged trees during severe snow storm in January 2008 (Zhou et al, 2010). The damaged trees lowered the plant transpiration in summer, and hence lowered ET and ET/PET. PET in our CDR can be used to rule out these false droughts. Though radiation is the dominant limiting factor for vegetation growth in the Amazon (Nemani et al., 2003), the Amazon experienced the worst drought in 40 years during 2005 (Hopkin, 2005), and water became the dominant limiting factor (Phillips et al., 2009; Zhao and Running, 2010). Combining global MOD16 ET/PET and MOD13A2 NDVI products, Mu et al. (2013) developed a MODIS global terrestrial drought severity index to monitor and detect droughts and to help the decision makers to mitigate the adverse effects from droughts.

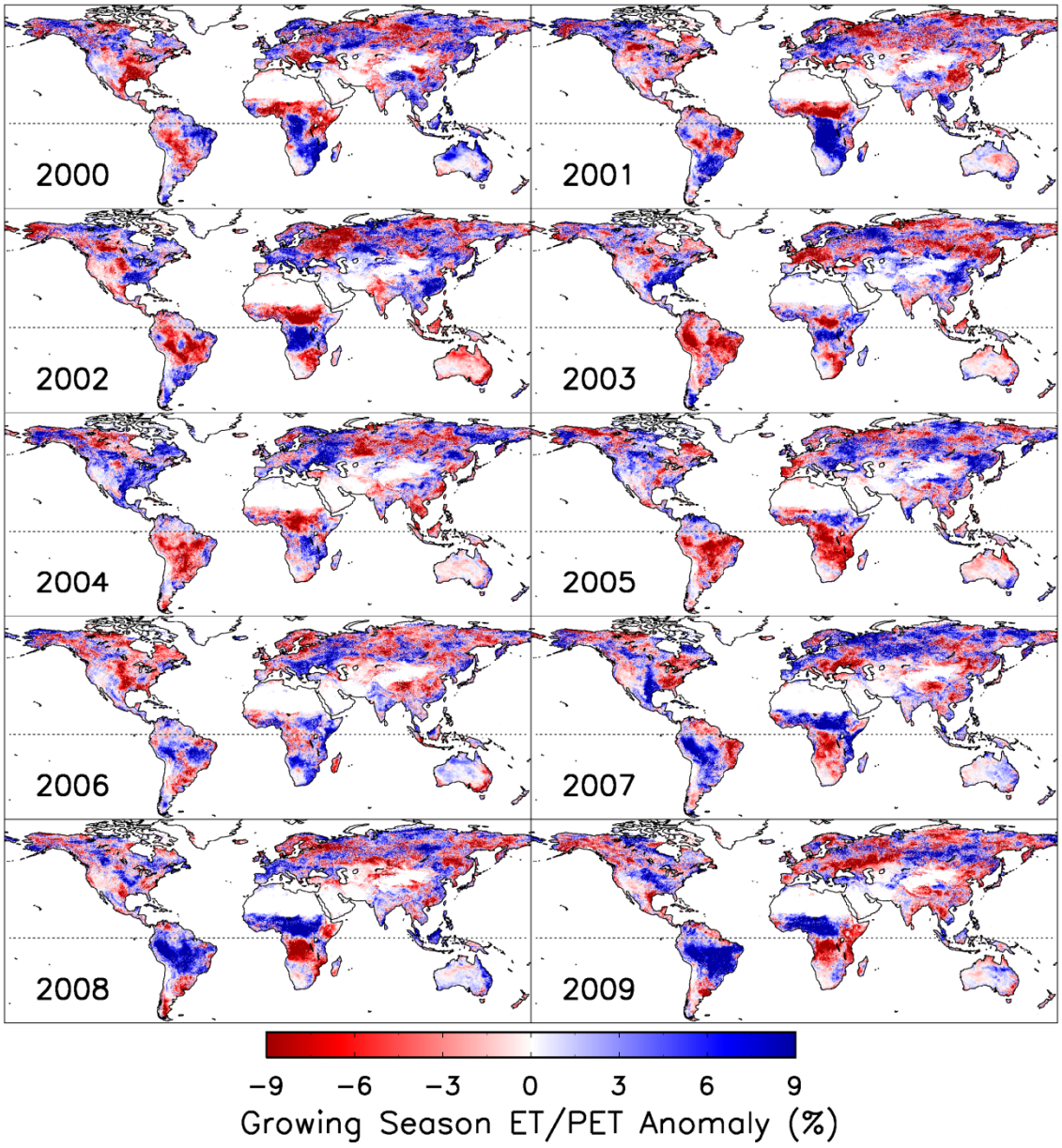

Figure 11 Spatial pattern of global MODIS ET to PET ratio anomalies during 2000-2009. Large-scale ET/PET negative anomalies were mainly caused by droughts.

6.3 Algorithm Performance at Global Watersheds

As a different more spatially integrated evaluation, we obtained the stream flow data at global watersheds (Dai et al., 2009). Theoretically, over a relatively long time period, gauged catchment ET can be roughly estimated as the difference between precipitation and stream flow by assuming that there is no change in soil water storage (Budyko, 1974; Donohue et al., 2007).

The average annual gridded precipitation data of Chen et al (2002) and the Global Precipitation Climatology Centre (Rudolf and Schneider, 2005) was subtracted by stream flow to get pseudo ET observations (ET OBS) for the watersheds. 232 watersheds having at least five years of water discharge data were used to do the comparison (Fig. 12). Figure 12 shows the comparison of annual pseudo ET OBS from these 232 watersheds with the MODIS ET (driven by MERRA GMAO meteorology) averaged over each watershed over at least five years during 2000-2006. The MOD16 ET estimates can explain 85% of the variations of the pseudo ET observations for these 232 watersheds.

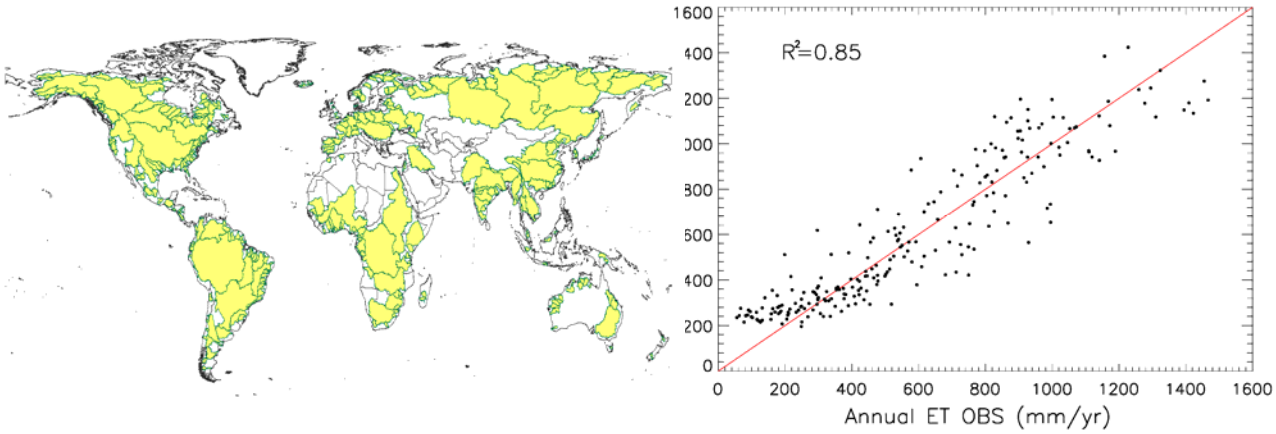

Figure 12 (Left) Distribution of the 232 watersheds used for validation of global MOD16 ET data. Each watershed is depicted in yellow. (Right) Comparison of annual pseudo ET observations (ET OBS, precipitation minus stream flow) from the 232 watersheds and the MODIS ET estimates averaged over each watershed over at least five years during 2000-2006. The runoff data for the watersheds were provided by Ke Zhang.

6.4 Uncertainties

The existing biases between the ET estimates and the ET measurements arises from below major causes,

1) Algorithm input data. MODIS LAI and FPAR (MOD15) are of the most important biophysical variables that control the exchange of energy, mass (e.g., water and CO_2) and momentum between the earth surface and atmosphere (Dickinson et al., 1993; Sellers et al., 1996; Tian et al., 2004; Demarty et al., 2007). However, there are uncertainties in MODIS LAI/FPAR retrievals, for example, MODIS LAI tends to be higher and the growing season is too long over boreal forests (Demarty et al., 2007). MODIS LAI validation suggests three key factors that influence the accuracy of LAI retrievals: 1) uncertainties in input land cover data, 2) uncertainties in input surface reflectance, and 3) uncertainties from the model used to build the look-up tables accompanying the algorithm (Yang et al., 2006). Mu et al. (2012) analyzed the variance and uncertainty in MOD16 ET driven by three different meteorological datasets, GMAO, ECMWF and NCEP1. MOD16 ET driven by GMAO has more detailed spatial ET variations than the other two, largely because first, GMAO has the finest resolution (1.00°x1.25°) among the three meteorological datasets, and second, overall, GMAO has the best quality at the global scale, except for its low radiation in equatorial regions. Heinsch et al. (2006) compared tower meteorological

data with GMAO data, and the 1-km^2 Collection 4 MODIS LAI (MOD15) and MODIS land cover (MOD12) with ground-based measurements, finding existing biases in both the GMAO data and the MODIS data when compared to observations. While approximately 62% of MODIS LAI estimates were within the estimates based on field optical measurements, remaining values overestimated site values (Heinsch et al., 2006). Comparison of LAI at the patch level can significantly improve the agreements, but the Collection 3 MODIS LAI still tends to be higher (Wang et al., 2004). Overestimates of LAI may result in overestimates of ET even if other input data such as the meteorological data and MODIS albedo data are relatively accurate. Although the temporal filling of unreliable MODIS data, including LAI, FPAR and albedo, greatly improves the accuracy of inputs, the filled values are artificial and contain uncertainties. There is a hypothesis that all the uncertainties associated with the MODIS data are contained in the quality flags MODIS QA, an assumption which proved efficient for reducing the weight of unreliable satellite products, especially over tropical forests (Demarty et al., 2007). However, the MODIS QA remains a qualitative measure of uncertainty, and does not quantitatively accounts for each source of error in the MODIS data retrieval procedure (sensor calibration, atmospheric corrections, land cover mapping radiative transfer forward and inverse modelling) (Demarty et al., 2007). Also, the inaccuracy in MODIS FPAR will lead to miscalculation of Fc, and hence ET. All of these uncertainties from inputs can introduce biases in ET estimates that are difficult to detect.

2) Inaccuracy in the measured data. Currently, the ground data from the eddy covariance flux towers provide the best ET estimates. However, they have an error or uncertainties of about 10-30% based on comparison of multiple towers at the same site, or by comparison with independent measurements of ET by other methods such as lysimeters or sap flux sensors (Glenn et al., 2008b). Also, the eddy covariance flux towers have an energy balance closure problem that, the sum of the net radiation and the ground heat flux, was found in most cases to be larger than the sum of turbulent fluxes of latent heat and sensible heat (Aubinet et al., 2000; Wilson et al., 2002). Correcting error and reducing uncertainty in the ET measurements are still uncertain due to the closure error (Shuttleworth, 2007). Scott (2010) used the watershed water balance to evaluate the accuracy of eddy covariance ET measurements at three semiarid ecosystems, and found that eddy covariance towers usually underestimated the ET at high values and overestimated the ET at the low values.

3) Scaling from tower to landscape. The measuring height and the horizontal scale of measurement of the turbulent fluxes like latent heat fluxes and sensible heat fluxes, usually 2-5m, have significant influences on the footprint (Schmid, 1997) and the size of underlying surface (Foken, 2008). Also, the complex terrain (Aubinet et al., 2005; Feigenwinter et al., 2008) and complicated canopy structure, the stochastic nature of turbulence (Hollinger and Richardson, 2005; Moncrieff et al., 1996) can affect the eddy covariance measurements (Yi et al., 2010). The comparison of measured ET with the estimated from the 3×3 1-km^2 MODIS across all 46 sites may introduce uncertainties due to the differences in tower footprints for different towers and under varying environmental conditions for a given tower. For example, among the 46 towers used to examine the performance of the ET algorithms, there are seven eddy covariance towers at MB, Canada (CANS1…7), which are very close and are all ENF (Table 5). The ET measurements at the seven CANS towers are quite different, with the average daily ET ranging from 0.38 to 0.59 mm day^{-1} (Table 7). The magnitudes and interannual variability substantially differ among the seven CANS towers. And in heterogeneous areas, the differing scales of the tower and MODIS ET estimates should be performed via an upscaling process, such as that used during the Bigfoot

MODIS validation project (Cohen et al., 2003; Turner et al., 2003a, 2003b). The expense and intensity of such studies, however, limits our ability to perform such comparisons.

4) Algorithm limitations. A large number of physical factors are involved in soil surface evaporation and plant transpiration processes, including microclimate, plant biophysics for site specific species and landscape heterogeneity, making accurate assessment of ET a challenge (Friedl, 1996; Vörösmarty, et al., 1998; McVicar et al, 2007). Some issues remaining in the ET algorithm may contribute to the differences between the tower ET measurements and the ET estimates by the algorithm. The algorithm doesn't account for the stand age, disturbance history or species composition. Biophysical parameters such as *gl_sh*, rbl_{max} and rbl_{min}, VPD_{open} and VPD_{close} used in the algorithm have uncertainties since the same values are used for a given biome type globally. We have little knowledge regarding some parameters (e.g., the soil heat fluxes, the boundary layer resistance for soil evaporation) and the mechanisms involved. Although it is generally assumed that stomata close at night, several studies have documented nighttime stomatal opening in many species over a range of habitats (Musselman and Minnick 2000). Incomplete stomatal closure during the night is observed in a diverse range of vegetation types (Daley and Phillips, 2006; Caird et al., 2007; Zeppel et al., 2010). Assumption of the stomata closure at night can induce biases to the nighttime plant transpiration, and hence induce underestimated daily total ET. Increasing CO_2 content tends to reduce plant transpiration due to a high-CO_2 induced partial stomatal closure (Idso and Brazel, 1984). Within one or two decades, this effect on ET may be negligible; however, as data record lengthening, this effect is needed to account for. As a result, theoretically, we may overestimate ET. We will add antitranspiration effect from enriched CO_2 to the transpiration module in our algorithm when we study the long-term remotely sensed ET changes.

7. MOD16 Products

This section details MOD16 variables, data file format, map projection, file name, and size.

7.1 MOD16 Variables

The 8-day ET (0.1mm/8days for the 8-day before the last 8-day of a year or 0.1mm/5days for the last 8-day) is the sum of ET during these 8-day time periods (5 days for 361 composite data in regular years and 6 days for a leap year). The monthly ET (0.1mm/month) is the sum of monthly ET. For February, there are 29 days in a leap year and 28 days in regular years. The annual ET (0.1mm/yr) is the sum of the ET during each year. There are 366 days in 2000, 2004, 2008, and 365 days in 2001, 2002, 2003, 2005, 2006, 2007, 2009, and 2010. The 8-day, monthly and annual latent heat flux (LE)/potential LE (PLE) (10^{-4} J/m^2/day) is the average daily LE/PLE over the corresponding time period.

The users should multiply 0.1 to get the real ET/PET values in mm/8day or mm/month, or mm/yr, and 10^4 to get LE/PLE in J/m^2/day.

For the 8-day and monthly ET/LE/PET/PLE, annual LE/PLE, the valid value range is -32767-32700.

Fill value, out of the earth 32767
Water body 32766
Barren or sparsely vegetated 32765
Permanent snow and ice 32764
Permanent wetland 32763
Urban or Built-up 32762
Unclassified 32761

For the annual ET/PET, the valid value range is 0- 65500.

Fill value, out of the earth 65535
Water body 65534
Barren or sparsely vegetated 65533
Permanent snow and ice 65532
Permanent wetland 65531
Urban or Built-up 65530
Unclassified 65529

The MOD16 global evapotranspiration (ET)/latent heat flux (LE)/potential ET (PET)/potential LE (PLE) datasets are regular 1-km^2 land surface ET datasets for the 109.03 Million km^2 global vegetated land areas at 8-day, monthly and annual intervals. The dataset covers the time period 2000 – 2010. Future years will be produced and posted periodically, but not in near-real time.

The output variables include, 8-day, monthly and annual ET, LE, PET, PLE and 8-day, annual quality control (ET_QC). The 8-day MOD16A2 QC field is inherited from MOD15A2 in the same period. However, the cloud-contaminated FPAR/LAI has been temporally filled with those having good QC. For annual QC of MOD16A3 products, we used the method proposed by Zhao et al. (2005) to define a more meaningful annual ET QC as

$$\mathrm{QC} = 100.0 \times \mathrm{NU_g}/\mathrm{Total_g}$$

where NUg is the number of days during growing season with unreliable or missing MODIS LAI inputs, and Totalg is total number of days in the growing season. The growing season is defined as all days with Tmin above the value where stomata close as in the BPLUT. The MOD16 ET algorithm has a good performance in generating global ET data products, providing critical information on global terrestrial water and energy cycles and environmental changes (Mu et al., 2007, 2009, 2011).

7.2 MOD16 HDFEOS 10-degree Tiles, Map Projection and File Name

As a level 4 MODIS data product, the MOD16 global ET dataset follows the high level of global MODIS data structure and file format. The data are saved in HDFEOS (Hierarchical Data Format - Earth Observing System) file format with Sinusoidal map projection, an equal-area global map projection. As shown in Figure 13, the globe is divided into 36 (horizontal direction) by 18 (vertical direction) tiles with each tile called a MODIS “10-degree” tile. For MODIS land products, there are 317 tiles with land pixels. For MOD16 ET, similar to the level

3 FPAR/LAI and level 4 MODIS GPP/NPP data products, we further exclude 31 tiles with no vegetated pixels. These excluded 31 tiles are located in high latitudes beyond 80˚N and 60˚S.

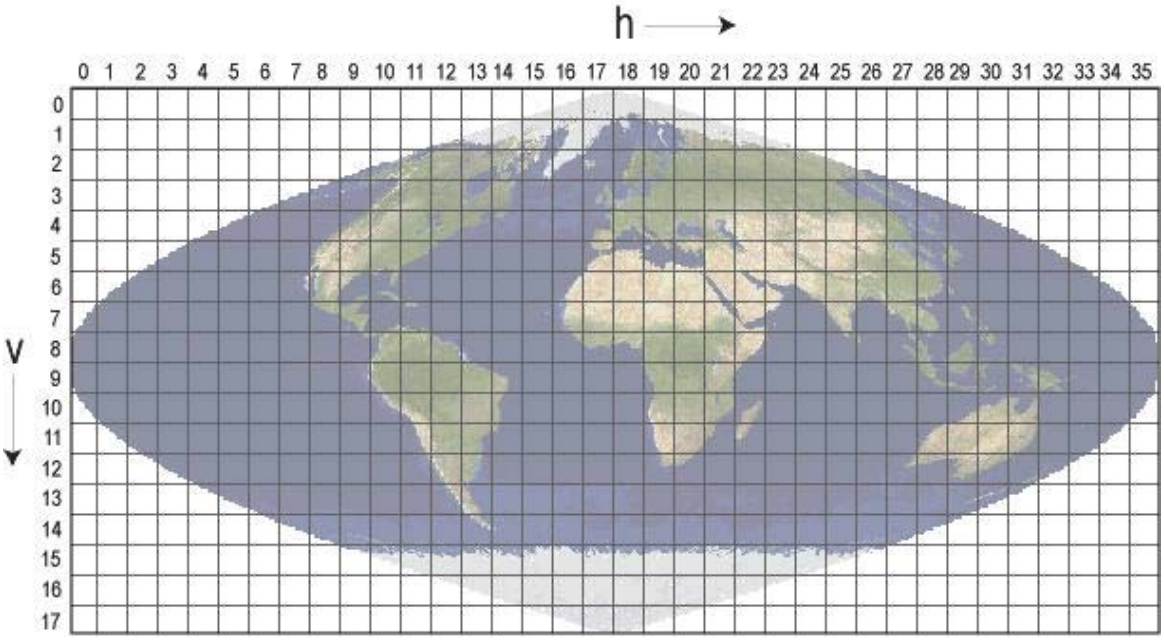

Figure 13 MODIS Sinusoidal "10-degree" tile system. For land data products, there are 317 tiles with land pixels, of which 286 tiles with vegetated pixels located between 60˚S to 80˚N.

The MOD16 file name has the same naming style as other high level of MODIS data products. For example, the filename MOD16A2.A2002081.h02v06.105.2010355155223.hdf indicates:

- MOD16A2 - Product Short Name
- .A2002081 - Julian Date of Data Acquisition (A-YYYYDDD)
- . h02v06 - Tile Identifier (horizontalXXverticalYY)
- .105 - Collection Version
- . 2010355155223 - Julian Date and time of being generated (YYYYDDDHHMMSS)
- .hdf - Data Format (HDF-EOS)

For a nominal "1-km" MODIS ET, it has 1200 by 1200 pixels in a tile and the real spatial resolution for a pixel is [(10 / 1200) / 180] * Pi * 6371007.181 = 926.6254331 meters, and here 6371007.181 meters is the earth radius used by MODIS Sinusoidal map projection.

MOD16 products have only one sources of metadata: the embedded HDF metadata. The HDF metadata contains valuable information including global attributes and data set-specific attributes pertaining to the granule. Some key features of certain MODIS metadata attributes include the following:

• The XDim and YDim represent the rows and columns of the data, respectively
• The Projection and ProjParams identify the projection and its corresponding projection parameters. The value of projection is GCTP_SNSOID. The 1-dimentioanl array of

ProjParams contains other parameters for map projection. The first value 6371007.181000 is the earth radius used by MODIS high level data products.
• The UpperLeftPointMtrs is in projection coordinates, and identifies the very upper left corner of the upper left pixel of the image data
• The LowerRightMtrs identifies the very lower right corner of the lower right pixel of the image data. These projection coordinates are the only metadata that accurately reflect the extreme corners of the gridded image
• There are additional BOUNDINGRECTANGLE and GRINGPOINT fields within the metadata, which represent the latitude and longitude coordinates of the geographic tile corresponding to the data

The Data Set attributes contain specific SDS information such as the data range and applicable scaling factors for the data. An HDF-EOS file also contains EOS core metadata essential for EOS search services.

Currently, there is some free or commercial software able to deal with MODIS HDFEOS files, such as MODIS Reprojection Tool (MRT), HDF-EOS to GeoTIFF converter (HEG), IDL/ENVI, ERDAS etc.

7.3 MOD16 Product Data Size

8-day MOD16A2

It contains five variables, including ET_1km, LE_1km, PET_1km, PLE_1km, ET_QC_1km. The first four variables are in 2-byte short integer and the last one in 1-byte unsigned integer. Therefore, the five variables have nine bytes. Then in theory, for a one year (46 8-day) 286 tiles 1-km global data, they will have a size equal to 9 * 1200 * 1200 * 286 * 46 = 0.17 TB. Thanks to the powerful capability of internal compression of HDF, only about 17% of size is required for the internal-zipped HDFEOS. As a result, **global 8-day MOD16A2 requires about 30 GB** for each year.

Monthly MOD16A2

It only contains ET_1km, LE_1km, PET_1km, PLE_1km which have the same data types as the corresponding four variables as in the 8-day MOD16A2 product. In theory, for one year, total data size should be 8 * 1200 * 1200 * 286 * 12 = 40 GB. After internal compression, about 20% of size is required, and **global monthly MOD16A2 requires about 8.1 GB** for each year.

Annual MOD16A3

It contains five variables, including ET_1km, LE_1km, PET_1km, PLE_1km, ET_QC_1km. The first four variables are in either singed or unsigned 2-byte short integer, and the last one is in unsigned one-byte integer. For one year, the data size should be 9 * 1200 * 1200 * 286 = 4 GB, and the internal compression results in **0.9 GB of global MOD16A3** for each year.

In all, for each year, MOD16 ET product requires 30 + 8.1 + 0.9 = 39 GB. For 11 years from 2000 through 2010, there are totally about 429 GB data for the global MOD16

A2/A3 product. Note that we haven't mentioned the space of all the input datasets to the global MOD16 algorithm, which are detailed in section 4 above.

8. Summary

Table 8. 321 users from 38 countries requesting MODIS ET/PET/LE data over 2006-2012. N: number of users.

N	Country	N	Country	N	Country	N	Country	N	Country
20	Australia	2	Czech Republic	2	Iran	1	Poland	5	Switzerland
1	Azerbaijan	1	Columbia	3	Italy	1	Portugal	1	Thailand
1	Argentina	5	Denmark	2	Japan	1	North Africa	1	Tunisia
4	Austria	3	Ethiopia	1	Mexico	7	S. Africa	12	UK
2	Belgium	8	France	1	New Zealand	8	S. Korea	144	USA
6	Brazil	1	Bolivia	1	Nepal	3	Spain	1	W. Africa
8	Canada	10	Germany	11	Netherlands	2	Sri Lanka		
22	China	13	India	1	Peru	5	Sweden		

ET from the land surface is a key water cycle variable which is directly related to energy budgets, water cycle, daily meteorology and climate, and ecosystem carbon fluxes. Terrestrial ecosystems are an inherent participant in the surface water cycle and energy exchange, and thus ET is also a metric of ecosystem services, functions and status of ecosystem health. With climate change, the frequency, intensity and duration of droughts have increased (Zhao and Running, 2010; Dai, 2011; Mu et al., 2013). There is a strong demand for regular regional and global ET products at satellite sensor's spatial resolution from the scientific community, land managers and policy makers for the purposes of water management and environmental monitoring. Extensive activities have been carried out to validate the MOD16 product at different ecosystems globally with results having been and being published. Evaluating the performance of MOD16 ET algorithm at tower site level, watershed level and globally verifies the reliability of the MOD16 ET product (Ruhoff et al., 2012; Xia et al., 2012). High-resolution land surface water and energy balances are greatly desired by vast users. MOD16 ET dataset has been widely used by different communities and got some very interesting scientific findings, with one published in *Nature* and another on *Nature Climate Change* (Montenegro et al., 2009; Jung et al., 2010; Loarie et al., 2011; Lathuillière et al., 2012; Mu et al., 2011b; Sun et al., 2011). There had been 268 scientists from 32 countries contacting us for using MOD16 ET data over 2000-2012, even though we released the data to the public in Jan. 2011 (Table 8). Now MOD16 ET data is ready for users to download and answer relevant environmental questions.

9. References

Allen, R.G., M. Tasumi, A. Morse, R. Trezza, J.L. Wright, W. Bastiaanssen, W. Kramber, I. Lorite, C.W. Robison (2007). Satellite-Based Energy Balance for Mapping Evapotranspiration with Internalized Calibration (METRIC)—Applications. *Journal of Irrigation and Drainage Engineering* 33(4): 395-406.

Anthoni, P.M., M.H. Unsworth, B.E. Law, J. Irvine, D. Baldocchi, D. Moore (2002). Seasonal differences in carbon and water vapor exchange in young and old-growth ponderosa pine ecosystems. *Agricultural and Forest Meteorology* 111:203-222.

Asner, G. P., J. M. O. Scurlock, J. A. Hicke (2003). Global synthesis of leaf area index observations: Implications for ecological and remote sensing studies. *Global Ecology and Biogeography*, 12(3), 191−205. doi:10.1046/j.1466-822X.2003.00026.x

Aubinet, M. (2000). Estimates of the annual net carbon and water exchange of forests: the EUROFLUX methodology. *Adv. Ecol. Res*. 30, 113–175.

Aubinet, M., P. Berbigier, C. Bernhofer, et al. (2005). Comparing CO_2 storage and advection conditions at night at different CARBOEUROFLUX sites. *Boundary-Layer Meteorology* 116 (1): 63–93.

Baldocchi, D. D. (2008). Breathing" of the terrestrial biosphere: Lessons learned from a global network of carbon dioxide flux measurement systems. *Australian Journal of Botany* 56: 1-26.

Baldocchi, D.D., L. Xu, N. Kiang (2004). How plant functional-type, weather, seasonal drought, and soil physical properties alter water and energy fluxes of an oak-grass savanna and an annual grassland. *Agricultural and Forest Meteorology*, 123(1-2): 13-39.

Bastiaanssen, W. G. M., Menenti, M., Feddes, R. A., & Holtslag, A. A. M. (1998b). The Surface Energy Balance Algorithm for Land (SEBAL): Part 2 validation. *Journal of Hydrology*, 212–213: 213−229.

Bastiaanssen, W.G.M., E.J.M. Noordman, H. Pelgrum, G. Davids, B.P. Thoreson, R.G. Allen (2005). SEBAL model with remotely sensed data to improve water-resouces management under actual field conditions. *J Irrig Drain* 131: 85-93.

Bastiaanssen,W. G. M.,Menenti,M., Feddes, R. A., Holtslag, A. A. M. (1998a). A remote sensing surface energy balance algorithm for land (SEBAL): 1. Formulation. *Journal of Hydrology*, 212–213: 198−212.

Belward, A., J. Estes, et al. (1999). The IGBP-DIS Global 1-km Land-Cover Data Set DISCover: A Project Overview. *Photogrammetric Engineering & Remote Sensing* 65: 1013-1020.

Bouchet, R. J. (1963). Evapotranspiration re´elle evapotranspiration potentielle, signification climatique, pp. 134– 142, in *International Association of Scientific Hydrology, General Assembly of Berkeley, Transactions, vol. 2, Evaporation, Berkeley, Calif.*

Budyko, M. I. (1974). Climate and life, Academic, New York.

Caird, M.A., J.H. Caird, L.A. Caird (2007). Nighttime Stomatal Conductance and Transpiration in C3 and C4 Plants. *Plant Physiology* 143, 4-10

Chen, M., P. Xie, J.E. Janowiak, P.A. Arkin (2002). Global Land Precipitation: A 50-yr monthly analysis based on gauge observations. *Journal of Hydrometeorology* 3: 249−266.

Choudhury, B. J., N. E. DiGirolamo (1998). A biophysical process-based estimate of global land surface evaporation using satellite and ancillary data I. Model description and comparison with observations. *Journal of Hydrology* 205: 164−185.

Clark, K.L., H.L. Gholz, M.S. Castro (2004). Carbon dynamics along a chronosequence of slash pine plantations in north Florida. *Ecological Applications* 14:1154-1171.

Cleugh, H. A., R. Leuning, Q. Mu, S. W. Running (2007). Regional evaporation estimates from flux tower and MODIS satellite data. *Remote Sensing of Environment* 106, 285–304.

Clothier, B. E., K. L. Clawson, P. J. Jr. Pinter, M. S. Moran, R. J. Reginato, R. D. Jackson (1986). Estimation of soil heat flux from net radiation during growth of al~:alfa, *Agric. For. Meteorol.* 37:319-329.

Cohen, W. B., Maiersperger, T. K., Yang, Z., Gower, S. T., Turner, D. P., Ritts, W. D., et al. (2003). Comparisons of land cover and LAI estimates derived from ETM+ and MODIS for four sites in North America: A quality assessment of 2000/2001 provisional MODIS products. *Remote Sensing of Environment*, 88, 233−255.

Cook, B.D., K.J. Davis, W. Wang, A. Desai, B.W. Berger, R.M. Teclaw, J.G. Martin, P.V. Bolstad, P.S. Bakwin, C. yi, W. Heilman (2004). Carbon exchange and venting anomalies in an upland deciduous forest in northern Wisconsin, USA. *Agricultural and Forest Meteorology* 126: 271–295

Cook, E.R., R. Seager, M.A. Cane, D.W. Stahle (2007) North American drought: Reconstructions, causes, and consequences. *Earth-Science Reviews* 81 (1-2): 93–134.

Courault, D., B. Seguin, A. Olioso (2005). Review on estimation of evapotranspiration from remote sensing data: From empirical to numerical modeling approaches. *IRRIG DRAIN System* 19: 223-249.

Courault, D., B. Sequin, A. Olioso (2005). Review on estimation of evapotranspiration from remote sensing data: From empirical to numerical modeling approaches. *Irr Drain Syst* 19:223-249.

da Rocha, H.R., M.L. Goulden, S.D. Miller, M.C. Menton, L.D.V.O. Pinto, H.C. de Freitas, F. Silva, M. Adelaine (2004) Seasonality of water and heat fluxes over a tropical forest in eastern Amazonia. *ECOL APPL* 14 (sp4), 22-32.

Dai, A., 2011: Drought under global warming: A review. *Wiley Interdisciplinary Reviews: Climate Change*.

Dai, A., T. Qian, K. E. Trenberth, J. D Milliman (2009). Changes in continental freshwater discharge from 1948-2004. *J. Climate*, **22**, 2773-2791.

Daley, M.J., N.G. Phillips (2006) Interspecific variation in nighttime transpiration and stomatal conductance in a mixed New England deciduous forest. *Tree Physiology* 26, 411–419.

Dang, Q.L., H.A. Margolis, M.R. Coyea, M. Sy, G.J. Collatz (1997). Regulation of branch-level gas exchange of boreal trees: roles of shoot water potential and vapour pressure difference. *Tree Physiology* 17: 521-535.

Daughtry, C.S.T., W.P. Kustas, M.S. Moran, P.J. Jr. Pinter, R.D. Jackson, P. W. Brown, W. D. Nichols, L. W. Gay (1990). Spectral Estimates of Net Radiation and Soil Heat Flux. *Remote Sensing of Environment* 32: 111-124.

Dawson, T.E., S.S. Burgess, K.P. Tu, R.S. Oliveira, L.S. Santiago, J.B. Fisher, K.A. Simonin, A.R. Ambrose (2007). Nighttime transpiration in woody plants from contrasting ecosystems. *Tree Physiol.* 27(4):561-75.

Demarty, J., F. Chevallier, A.D. Friend, N. Viovy, S. Piao, P. Ciais (2007). Assimilation of global MODIS leaf area index retrievals within a terrestrial biosphere model. *Geophysical Research Letters*, 34, L15402.

Desai, A.R., P.V. Bolstad, B.D. Cook, K.J. Davis, E.V. Carey (2005). Comparing net ecosystem exchange of carbon dioxide between an old-growth and mature forest in the upper Midwest, USA. *Agricultural and Forest Meteorology* 128(1-2): 33-55.

Dickinson, R.E., A. Hendersen-Sellers, P.J. Kennedy, M.F. Wilson (1993). Biosphere-Atmosphere Transfer Scheme (BATS) Version le as Coupled to the NCAR Community Climate Model. *CLIMATE AND GLOBAL DYNAMICS DIVISION*. BOULDER, CO. NCAR/TN-387+STR.

Donohue, R.J., M.L. Roderick, T.R. McVicar (2007). On the importance of including vegetation dynamics in Budyko's hydrological model. Hydrol. *Earth Syst. Sc*. 11: 983−995.

Engstrom, R., A. Hope, H. Kwon, Y. Harazono, M. Mano, W. Oechel (2006). Modeling evapotranspiration in Arctic coastal plain ecosystems using a modified BIOME-BGC model, *J. Geophys. Res.* 111, G02021

Fan, S., C. Chan-Kang, K. Qian, K. Krishnaiah (2003) National and international agricultural research and rural poverty: the case of rice in India and China. EPTD Discussion Paper No. 109. Washington, D.C.: Environment and production technology division. *International Food Policy Research Institute*.

Feigenwinter, C., C. Bernhofe, U. Eichelmann, et al. (2008). Comparison of horizontal and vertical advective CO_2 fluxes at three forest sites. *Agricultural and Forest Meteorology* 148 (1): 12–24.

Fisher, J. Y. Malhi , D. Bonal , H.R. da Rocha , A. de Araújo, Gamo, M, M. Goulden , T. Hirano , Huete, AR; Kondo, H; T. Kumagai , H. Loescher , S. Miller , A. Nobre , Y. Nouvellon, S. Oberbauer, S. Panuthai, O. Roupsard, S. Saleska , K. Tanaka, N. Tanaka, K.P. Tu, C. von Randow (2009). The land-atmosphere water flux in the tropics. *Global Change Biology*. 15 (11): 2694-2714.

Fisher, J.B., K. Tu, D.D. Baldocchi (2008). Global estimates of the land atmosphere water flux based on monthly AVHRR and ISLSCP-II data, validated at FLUXNET sites. *Remote Sensing of Environment* 112 (3): 901-919.

Fisher, J.B., T.A. DeBiase, Y. Qi, M. Xu, A.H. Goldstein (2005) Evapotranspiration models compared on a Sierra Nevada forest ecosystem. *Environmental Modelling & Software* 20: 783-796.

Foken, T. (2008). The energy balance closure problem: an overview. *Ecological Applications* 18 (6): 1351-1367.

French, A. N., F. Jacob, M. C. Anderson, W. P. Kustas, W. Timmermans, A. Gieske, Z. Su, H. Su, M F. McCabe, F. Li, J. Prueger, N. Brunsell (2005). Surface energy fluxes with the Advanced Spaceborne Thermal Emission and Reflection radiometer (ASTER) at the Iowa 2002 SMACEX site (USA). *Remote Sensing of Environment* 99: 55-65.

Friedl, M. A. (1996). Relationships among remotely sensed data, surface energy balance, and area-averaged fluxes over partially vegetated land surfaces. *Journal of Applied Meteorology*, 35, 2091−2103.

Friedl, M.A., D.K. McIver, J.C.F. Hodges, X.Y. Zhang, D. Muchoney, A.H. Strahler, et al. (2002). Global land cover mapping from MODIS: Algorithms and early results. *Remote Sensing of Environment* 83(1–2): 287−302.

Gavilána, P., J. Berengena, R.G. Allen (2007). Measuring versus estimating net radiation and soil heat flux: Impact on Penman–Monteith reference ET estimates in semiarid regions. *AGR WATER MANAGE* 89:275-286.

Gholz, H.L. K.L. Clark (2002). Energy exchange across a chronosequence of slash pine forests in Florida. *Agricultural and Forest Meteorology* 112:87-102.

Glenn, E.P., A.R. Huete, P.L. Nagler, S.G. Nelson (2008a). Relationship between remotely-sensed vegetation indices, canopy attributes and plant physiological processes: What vegetation indices can and cannot tell us about the landscape. *Sensors* 8: 2136-2160.

Glenn, E.P., K. Morino, K. Didan, F. Jordan, K.C. Carroll, P.L. Nagler, K. Hultine, L. Sheader, J. Waugh (2008b). Scaling sap flux measurements of grazed and ungrazed shrub communities with fine and coarse-resolution remote sensing. *Ecohydrology* 1 (4):316-329.

Global Modeling and Assimilation Office (2004). File specification for GEOSDAS gridded output version 5.3, report. Greenbelt, Md: NASA Goddard Space Flight Cent.

Granger R.J., D.M. Gray (1989). Evaporation from natural nonsaturated surfaces. *Journal of Hydrology* 111: 21-29.

Hadley, J.L., P.S. Kuzeja, M.J. Daley, N.G. Phillips, S. Singh, T. Mulcahy (2008). Water use and carbon exchange of eastern hemlock (Tsuga canadensis L.) and deciduous forests in the northeastern U.S.: Implications for ecosystem-level effects of the hemlock woolly adelgid. *Tree Physiology* 28: 615-627.

Hansen, M., R. DeFries, et al. (2000). Global land cover classification at the 1km spatial resolution using a classification tree approach. *International Journal of Remote Sensing* 21: 1331-1364.

Harazono, Y., M. Yoshimoto, A. Miyata, Y. Uchida, G.L. Vourlitis, W.C. Oechel (1995). Micrometeorological Data and Their Characteristics Over the Arctic Tundra at Barrow, Alaska during the Summer of 1993. Miscellaneous publication of the National Institute of Agro-Environmental Sciences No. 16, Japan 213 pp.

Heinsch, F.A., M. Zhao, S.W. Running, J.S. Kimball, R.R. Nemani, K.J. Davis, P.V. Bolstad, B.D. Cook, A.R. Desai, D.M. Ricciuto, B.E. Law, W.C. Oechel, H. Kwon, H. Luo, S.C. Wofsy, A.L. Dunn, J.W. Munger, D.D. Baldocchi, L. Xu, D.Y. Hollinger, A.D. Richardson, P.C. Stoy, M.B.S. Siqueira, R.K. Monson, S.P. Burns, L.B. Flanagan (2006). Evaluation of remote sensing based terrestrial productivity from MODIS using AmeriFlux tower eddy flux network observations. *IEEE Transactions on Geoscience and Remote Sensing*, 44(7): 1908-1925.

Hollinger, D.Y., A.D. Richardson (2005). Uncertainty in eddy covariance measurements and its application to physiological models. *Tree Physiol*. 25: 873–885.

Hope, A.S., R. Engstrom, D.A. Stow (2005). Relationship between AVHRR surface temperature and NDVI in arctic tundra ecosystems. *International Journal of Remote Sensing*, 26(8): 1771-1776.

Hopkin, M. (2005). Amazon hit by worst drought for 40 years. Nature News online 11 October 2005, *Nature*.

Horridge, M., J. Madden, G. Wittwer (2005) The impact of the 2002–2003 drought on Australia. *Journal of Policy Modeling*, 27: 285-308.

Huete A.R., K. Didan, Y.E. Shimabukuro, P. Ratana, S.R. Saleska, L.R. Hutyra, W. Yang, R.R. Nemani, R. Myneni (2006). Amazon rainforests green-up with sunlight in dry season, *Geophysical Research Letters* 33, L06405.

Hutyra, L.R., J.W. Munger, S.R. Saleska, E. Gottlieb, B.C. Daube, A.L. Dunn, D.F. Amaral, P.B. de Camargo, S.C. Wofsy (2007). Seasonal controls on the exchange of carbon and water in an Amazonian rainforest, *J. Geophys. Res, Biogeosciences*, 112: G03008.

Idso, S. B., A. J. Brazel (1984). Rising atmospheric carbon dioxide concentrations may increase streamflow. *Nature*, 312: 51-53.

Jacobsen, A., B.U. Hansen (1999). Estimation of the soil heat ¯ ux/ net radiation ratio based on spectral vegetation indexes in high-latitude Arctic areas. *int. j. remote sensing*, 20 (2): 445-461.

Jarvis, P.G. (1976). The interpretation of the variations in leaf water potential and stomatal conductance found in canopies in the field. *Philosophical Transactions of the Royal Society of London Series B* 273: 593–510.

Jenkins, J.P., A.D. Richardson, B.H. Braswell, S.V. Ollinger, D.Y. Hollinger, M.L. Smith (2007). Refining light-use efficiency calculations for a deciduous forest canopy using simultaneous tower-based carbon flux and radiometric measurements. *Agricultural and Forest Meteorology* 143 (1-2): 64-79.

Jiang, L., S. Islam, T. Carlson (2004). Uncertainties in latent heat flux measurement and estimation: implications for using a simplified approach with remote sensing data. *Can J Rem Sens* 30:769-787.

Jin, Y., C.B. Schaaf, C.E. Woodcock, F. Gao, X. Li, A.H. Strahler, et al. (2003). Consistency of MODIS surface BRDF/Albedo retrievals: 1. Algorithm performance. *Journal of Geophysical Research* 108(D5): 4158.

Jones, H. G. (1992). Plants and microclimate: a quantitative approach to environmental plant physiology. *Cambridge, UK: Cambridge University Press*.

Jung, M., M. Reichstein, P. Ciais, S.I. Seneviratne, J. Sheffield, M. L. Goulden, G. B. Bonan, A. Cescatti, J. Chen, R. de Jeu, A. J. Dolman, W. Eugster, D. Gerten, D. Gianelle, N. Gobron, J. Heinke, J. S. Kimball, B. E. Law, L. Montagnani, Q. Mu, B. Mueller, K. W. Oleson, D. Papale, A. D. Richardson, O. Roupsard, S. W. Running, E. Tomelleri, N. Viovy, U. Weber, C. Williams, E. Wood, S. Zaehle and K. Zhang (2010). Recent decline in the global land evapotranspiration trend due to limited moisture supply. *Nature* 467: 951-954.

Justice, C. O., Townshend, J. R. G., Vermote, E. F., Masuoka, E., Wolfe, R. E., Saleous, N., et al. (2002). An overview of MODIS Land data processing and product status. *Remote Sensing of Environment*, 83: 3−15.

Kaimal, J.C., J.J. Finnigan (1994). Atmospheric Boundary Layer Flows: Their Structure and Management. *Oxford University Press*, 289 pp.: New York.

Kalma, J.D., T.R. McVicar, M.F. McCabe (2008). Estimating land surface evaporation: A review of methods using remotely sensed surface temperature data. *Surv Geophys* 29:421-469.

Kawamitsu Y., S. Yoda, and W Agata (1993). Humidity pretreatment affects the responses of stomata and CO_2 assimilation to vapor pressure difference in C3 and C4 plants. *Plant cell physiology*, 34(1): 113-119.

Kelliher, F.M., R. Leuning, M.R. Raupach, E.D. Schulze (1995). Maximum conductances for evaporation from global vegetation types. *Agricultural and Forest Meteorology* 73 (1-2): 1-16.

Korzoun, V.I., A.A. Sokolov, M.I. Budyko, K.P. Voskresensky, G.P. Kalinin (1978). World water balance and water resources of the earth (English). In: Studies and Reports in Hydrology (UNESCO), no. 25 / United Nations Educational, Scientific and Cultural Organization, 75 - Paris (France); *International Hydrological Decade*, Moscow (USSR). *USSR National Committee* , 663 p.

Kustas, W., M. Anderson (2009). Advances in thermal infrared remote sensing for land surface modeling. *Ag For Meteor* 149:2071-2081.

Kustas, W.P., C.S.T. Daughtry (1990). Estimation of the soil heat flux/net radiation ratio from spectral data, *Agric. For. Meteorol.* 49:205-223.

Landsberg, J.J., S.T. Gower (1997). Applications of physiological ecology to forest management. *Academic Press*.

Law, B.E., E. Falge, L. Gu, D. D. Baldocchi, P. Bakwin, P. Berbigier, K. Davis, A. J. Dolman, M. Falk, J. D. Fuentes, A. Goldstein, A. Granier, A. Grelle, D. Hollinger, I. A. Janssens, P. Jarvis, N. O. Jensen, G. Katul, Y. Mahli, G. Matteucci, T. Meyers, R. Monson, W. Munger, W. Oechel, R. Olson, K. Pilegaard, K. T. Paw U, H. Thorgeirsson, R. Valentini, S. Verma, T. Vesala, K. Wilson, S. Wofsy (2002). Environmental controls over carbon dioxide and water vapor exchange of terrestrial vegetation. *Agricultural and Forest Meteorology* 113 (1-4): 97-120.

Lawrimore, J, R.R. Heim, M. Svoboda, et al. (2002) Beginning a new era of drought monitoring across North America. *Bulletin of the American Meteorological Society*, 83 (8): 1191-1192.

Leuning, R. (1995). A critical appraisal of a combined stomatal-photosynthesis model for C3 plants. *Plant, Cell and Environment* 18: 339–55.

Liski, J., A. Nissinen, M. Erhard, O. Taskinen (2003). Climatic effects on litter decomposition from Arctic tundra to tropical rainforest. *Global Change Biology* 9(4): 575−584.

Loarie, S. R., D. B. Lobell, G. P. Asner, Q. Mu, C. B. Field (2011). Direct impacts on local climate of sugarcane expansion in Brazil. *Nature Climate Change* 1 (2): 105-109.

Los, S. O., Collatz, G. J., Sellers, P. J., Malmstrom, C. M., Pollack, N. H., DeFries, R. S., et al. (2000). A global 9-yr biophysical land surface dataset from NOAA AVHRR data. *Journal of Hydrometeorology*, 1(2): 183-199.

L'vovich, M. I., G. F. White (1990). Use and transformation of terrestrial water systems. Pages 235-252 in B. L. Turner II, W. C. Clark, R. W. Kates, J. F. Richards, J. T. Mathews, and W. B. Meyer, editors. The Earth as transformed by human action. *Cambridge University Press, Cambridge*, UK.

Maidment, D.R. (1993). Handbook of Hydrology. Publisher: *McGraw-Hill*.

Malhi, Y. T.R. Baker, O.L. Phillips, S. Almeida, E. Alvarez, L. Arroyo, J. Chave, C.I. Czimczik, A. Di Fiore, N. Higuchi, T.J. Killeen, S.G. Laurance, W.F. Laurance, S.L. Lewis, L.M.M. Montoya, A. Monteagudo, D.A. Neill, P.N. Vargas, S. Patiño, N.C.A. Pitman, C.A. Quesada, R. Salomão, J.N.M. Silva, A.T. Lezama, R.V. Martínez, J. Terborgh, B. Vinceti, J. Lloyd (2004) The above-ground coarse wood productivity of 104 Neotropical forest plots. *GLOBAL CHANGE BIO*L 10 (5), 563–591.

Malhi, Y., D. Wood, T. R. Baker, J. Wright, O. L. Phillips, T. Cochrane, et al. (2006). The regional variation of aboveground live biomass in old growth Amazonian forests. *Global Change Biology*, 12(7), 1107−1138. doi:10.1111/j.1365-2486.2006.01120.x

Marsden, B.J., V.J. Lieffers, J.J. Zwiazek (1996). The effect of humidity on photosynthesis and water relations of white spruce seedlings during the early establishment phase. *Can. J. For. Res.* 26: 1015-1021.

McCabe, M.F., E.F. Wood (2006). Scale influences on the remote estimation of evapotranspiration using multiple satellite sensors. *Remote Sensing of Environment* 105: 271-285.

McVicar, T.R., T.G. Van Niel, L. Li, E.A. King, R.J. Donohue (2007). Deriving moisture availability from time series remote sensing for ecohydrological applications:

Development of a prototype near real-time operational system. *CSIRO Land and Water Science Report* 37/07.

Mecikalski, J.R., G.R. Diak, M.C. Anderson, J.M. Norman (1999). Estimating fluxes on continental scales using remotely sensed data in an atmospheric-land exchange model. *J APPL METEOROL* 38: 1352-1369.

Mellouli, H.J., B. van Wesemael, J. Poesen, R. Hartmann (2000). Evaporation losses from bare soils as influenced by cultivation techniques in semi-arid regions. *Agricultural Water Management* 42 (3): 355-369.

Misson L., J.A. Panek, A.H. Goldstein (2004). A comparison of three approaches to modeling leaf gas exchange in annually drought-stressed ponderosa pine forests. *Tree Physiology*, 24: 529-541.

Moncrieff, J.B., Y. Malhi, R. Leuning (1996). The propagation of errors in long-term measurements of land-atmosphere fluxes of carbon and water. *Glob. Change Biol*. 2 (3): 231–240.

Monteith, J. L. (1965). Evaporation and environment. *Symposium of the society of experimental biology*, 19: 205−224.

Monteith, J. L. (1980). Principles of environmental physics. *Edward Arnold*.

Montenegro, A., M. Eby, Q. Mu, M. Mulligan, A. J. Weaver, E. C. Wiebe, M. Zhao (2009). The net carbon drawdown of small scale afforestation from satellite observations. *Global and Planetary Change* 69: 195-204.

Morton, F.I. (1983). Operational estimates of areal evapotranspiration and their significance to the science and pratice of hydrology. *J. Hydrol.*, 66:1-76.

Mu, Q., F.A. Heinsch, M. Zhao, S.W. Running (2007). Development of a global evapotranspiration algorithm based on MODIS and global meteorology data. *Remote Sensing of Environment*, 111, 519-536.

Mu, Q., L. A. Jones, J. S. Kimball, K. C. McDonald, S. W. Running (2009). Satellite assessment of land surface evapotranspiration for the pan-Arctic domain. *Water Resources Research*, Volume 45, Number W09420 – 2009.

Mu, Q., M. Zhao, F. A. Heinsch, M. Liu, H. Tian, S. W. Running (2007b). Evaluating water stress controls on primary production in biogeochemical and remote sensing based models. *Journal of Geophysical Research* 112, G01012.

Mu, Q., M. Zhao, J. S. Kimball, N. G. McDowell, S. W. Running (2013) A Remotely Sensed Global Terrestrial Drought Severity Index. *Bulletin of the American Meteorological Society*. DOI: 10.1175/BAMS-D-11-00213.1.

Mu, Q., M. Zhao, S. W. Running (2011). Improvements to a MODIS Global Terrestrial Evapotranspiration Algorithm. *Remote Sensing of Environment* 115: 1781-1800.

Mu, Q., M. Zhao, S. W. Running (2012) Remote Sensing and Modeling of Global Evapotranspiration. Chapter 19 in "Multiscale Hydrologic Remote Sensing: Perspectives and Applications", eds Chang, N., H. Yang. *Taylor and Francis Group*, p.443–479.

Mu, Q., M. Zhao, S.W. Running (2011b) Evolution of hydrological and carbon cycles under a changing climate. *Hydrological Processes* 25, 4093–4102. 25, 4093–4102.

Murray, F.W. (1967). On the computation of saturation vapor pressure, *J. Appl. Meteorol.* 6, 203–204.

Musselman, R.C., T.J. Minnick (2000). Nocturnal stomatal conductance and ambient air quality standards for ozone. *Atmos. Environ*. 34:719–733.

Myneni, R. B., S. Hoffman, Y. Knyazikhin, J.L. Privette, J. Glassy, Y. Tian, et al. (2002). Global products of vegetation leaf area and fraction absorbed PAR from year one of MODIS data. *Remote Sensing of Environment* 83(1–2): 214−231.

Nagler, P., J. Cleverly, D. Lampkin, E. Glenn, A. Huete, Z. Wan (2005). Predicting riparian evapotranspiration from MODIS vegetation indices and meteorological data. *Rem Sens Envir* 94: 17-30.

Nemani, R. R., C. D. Keeling, H. Hashimoto, W. M. Jolly, S. C. Piper, C. J. Tucker, R.B. Myneni, S. W. Running (2003). Climate-Driven Increases in Global Terrestrial Net Primary Production from 1982 to 1999. Science 300: 1560-1563.

Nemani, R.R., S.W. Running (1989). Estimation of Regional Surface Resistance to Evapotranspiration from NDVI and Thermal-IR AVHRR Data. *Journal of Applied Meteorology* 28: 276-284.

Nicholls, N. (2004) The changing nature of Australian droughts. *Climatic Change*, 63, 323-336.

Nishida, K., R.R. Nemani, J.M. Glassy, S.W. Running (2003a). Development of an evapotranspiration index from aqua/MODIS for monitoring surface moisture status. *IEEE Transactions on Geoscience and Remote Sensing* 41 (2): 493-501.

Nishida, K., R.R. Nemani, S.W. Running, J.M. Glassy (2003b). An operational remote sensing algorithm of land surface evaporation. *J. Geophys. Res*. 108(D9): 4270, doi:10.1029/2002JD002062.

Norman, J. M., W.B. Kustas, K.S. Humes (1995). Source approach for estimating soil and vegetation energy fluxes in observations of directional radiometric surface temperature. *Agricultural and Forest Meteorology* 77: 263−293.

Ogée, J., E. Lamaud, Y. Brunet, P. Berbigier and J. M. Bonnefond (2001). A long-term study of soil heat flux under a forest canopy. *AGR FOREST ENTOMOL* 106 (3): 173-186.

Oki, T., S. Kanae, (2006). Global Hydrological Cycles and World Water Resources, *Science* 313 (5790): 1068 – 1072.

Oren R., J.S., G.G. Katul, D.E. Pataki, B.E. Ewers, N. Phillips, K.V.R. Schäfer (1999). Survey and synthesis of intra- and interspecific variation in stomatal sensitivity to vapour pressure deficit. *Plant, Cell and Environment*, 22:1515-1526.

Oren, R., J.S. Sperry, B.E. Ewers, D.E. Pataki, N. Phillips, J.P. Megonigal (2001). Sensitivity of mean canopy stomatal conductance to vapor pressure deficit in a flooded Taxodium distichum L. forest: hydraulic and non-hydraulic effects. *Oecologia* 126: 21–9.

Overgaard, J., D. Rosbjereg, M. Butts (2006). Land-surface modeling in hydrological perspective – a review. *Biogeosci* 3: 229-241

Pandey, S., H. Bhandari, B. Hardy (2007) Economic costs of drought and rice farmers' coping mechanisms: a cross-country comparative analysis. *Los Baños, Laguna : IRRI*. 203 p.

Phillips, O.L., L.E.O.C. Aragão, S.L. Lewis, et al. (2009) Drought sensitivity of the Amazon rainforest. *Science* 323, 1344-1347.

Phillips, O.L., L.E.O.C. Aragao, S.L. Lewis, et al. (2009). Drought sensitivity of the Amazon rainforest. *Science* 323: 1344-1347.

Priestley, C.H.B., R.J. Taylor (1972). On the assessment of surface heat flux and evaporation using large scale parameters. *Monthly Weather Review* 100: 81–92.

Raupach, M.R. (2001). Combination theory and equilibrium evaporation. *Quarterly Journal of the Royal Meteorological Society* 127: 1149-1181.

Rocha H. R., A.O. Manzi , O. Cabral , S. Miller , M. Goulden , S. Saleska , N. Restrepo-Coupe , S. Wofsy , L. Borma, P. Artaxo, G. Vourlitis, J.S. Nogueira, F.L. Cardoso, A.D. Nobre, B. Kruijt, H.C. Freitas, C. von Randow, R.G. Aguiar, J.F. Maia (2009). Patterns of water and heat flux across a biome gradient from tropical forest to savanna in Brazil. J. Geophys. Res. – Biogeosciences, 114: G00B12.

Rosegrant, M.W., X. Cai, S.A. Cline (2003). Will the World Run Dry? Global Water and Food *Security. Environment: Where Science and Policy Meet* 45 (7).

Rudolf, B., U. Schneider (2005). Calculation of gridded precipitation for the global land-surface using in-situ gauge observations. *Proceedings of the 2nd Workshop of the International Precipitation Working Group*.

Ruhoff, A. L., A. R. Paz, L.E.O.C. Aragao, Q. Mu, Y. Malhi, W. Collischonn, H. R. Rocha, S. W. Running (2012) Assessment of the MODIS global evapotranspiration algorithm using eddy covariance measurements and hydrological modelling in the Rio Grande basin. *Hydrological Sciences Journal* (in press).

Running, S. W., J. S. Kimball (2005). Satellite-Based Analysis of Ecological Controls For Land-Surface Evaporation Resistance. *Encyclopedia of Hydrological Sciences*, M. Anderson (Ed.), *John Wiley & Sons*, Ltd. – 2005.

Running, S. W., R. R. Nemani, F. A. Heinsch, M. Zhao, M. C. Reeves. H. Hashimoto (2004). A continuous satellite-derived measure of global terrestrial primary production. *BioScience*, 54: 547–560.

Running, S.W., R.R. Nemani (1988). Relating seasonal patterns of the AVHRR Vegetation Index to simulate photosynthesis and transpiration of forests in different climates. *Remote sensing of Environment* 24: 347-367.

Salomon, J., C.B. Schaaf, A.H. Strahler, F. Gao, Y. Jin (2006). Validation of the MODIS Bidirectional Reflectance Distribution Function and Albedo Retrievals using combined observations from the aqua and terra platforms. *IEEE Transactions on Geoscience and Remote Sensing* 44(6): 1555-1565.

Sandford, A.P., P.G. Jarvis (1986). Stomatal responses to humidity in selected conifers. *Tree Physiology* 2: 89–103.

Scepan, J. (1999). Validation of High-Resolution Global Land-Cover Data Sets. *Photogrammetric Engineering & Remote Sensing* 65: 1051-1060.

Schaaf, C. B., F. Gao, A.H. Strahler, W. Lucht, X. Li, T. Tsang, et al. (2002). First operational BRDF, Albedo and Nadir Reflectance Products from MODIS. *Remote Sensing of Environment* 83: 135−148.

Schnid, H.P. (1997). Experimental design for flux measurements: matching scales of observations and fluxes. *Agricultural and Forest Meteorology* 87: 179-200.

Schubert, S., R. Rood, et al. (1993). An assimilated dataset for earth science applications. *Bulletin of the American Meteorological Society* 74: 2331-2342.

Schulze, E.D., F.M. Kelliher C. Körner J. Lloyd, R. Leuning (1994). Relationships among maximum stomatal conductance, ecosystem surface conductance, carbon assimilation rate and plant nitrogen nutrition: A global ecology scaling exercise. *Annit. Rev. Ecol. Syst.*, 25: 629-660.

Scott, R. L., (2010). Using watershed water balance to evaluate the accuracy of eddy covariance evaporation measurements for three semiarid ecosystems. *Agricultural and Forest Meteorology* 150: 219-225.

Sellers, P.J., D.A. Randall, G.J. Collatz, J.A. Berry, C.B. Field, D.A. Dazlich, et al. (1996). A revised land surface parameterization (SiB2) for atmosphere GCMs. Part II : The generation of global fields of terrestrial biophysical parameters from satellite data. *Journal of Climate* 9: 706−737.

Shuttleworth, W. J. (2007). Putting the "vap" into evaporation, *Hydrol. Earth Syst. Sci*. 11: 210-244.

Shuttleworth, W.J., J.S. Wallace (1985). Evaporation from sparse crops –An energy combination theory. *Quarterly Journal of the Royal Meteorological Society*, 111, 839−855.

Su, Z. (2002). The surface energy balance system (SEBS) (for estimation of turbulent heat fluxes. *Hydrology and Earth System Sciences*, 6: 85−99.

Su, Z. (2005). Hydrological applications of remote sensing: surface fluxes and other derived variables – surface energy balance. In *Encyclopedia of Hydrological Sciences*. (M. Anderson Ed.). John Wiley and Sons.

Sun, G., P. Caldwell, A. Noormets, S. G. McNulty, E. Cohen, J. Moore Myers, J.-C. Domec, E. Treasure, Q. Mu, J. Xiao, R. John, J. Chen (2011) Upscaling key ecosystem functions across the conterminous United States by a water-centric ecosystem model. *Journal of Geophysical Research*, Vol. 116, G00J05.

Tanaka, N., T. Kume, N. Yoshifuji, K. Tanaka, H. Takizawa, K. Shiraki, C. Tantasirin, N. Tangtham, M. Suzuki (2008). A review of evapotranspiration estimates from tropical forests in Thailand and adjacent regions. *AGR FOREST ENTOMOL* 148: 807–819.

Tasumi, M., R. Trezza, R. G. Allen, J. L. Wright (2005). Operational aspects of satellite-based energy balance models for irrigated crops in the semi-arid U.S. *IRRIG DRAIN System* 19: 355-376.

Taylor, K. E. (2001). Summarizing multiple aspects of model performance in a single diagram, *Journal of Geophysical Research* 106 (D7): 7183–7192.

Teuling, A.J., M. Hirschi, A. Ohmura, M. Wild, M. Reichstein, P. Ciasis, N. Buchmann, C. Ammann, L. Montagnani, A.D. Richardson, G. Wohifahrt, S.I. Seneviratne (2009). A regional prespective on trends in continental evaporation. *Geophys. Res. Lett.* 36, L02404

Thom, A.S. (1975). Momentum, mass and heat exchange of plant communities. In: Monteith, J. L. (ed.). *Vegetation and the Atmosphere*. Vol. 1. Principles. Pp. 57-109. London, Academic Press.

Thomas, C.K., B.E. Law, J. Irvine, J.G. Martin, J.C. Pettijohn, K.J. Davis (2009). Seasonal hydrology explains interannual and seasonal variation in carbon and water exchange in a semi-arid mature ponderosa pine forest in Central Oregon. *J Geophys. Res.* 114, G04006.

Thornton, P.E. (1998). Regional ecosystem simulation: combining surface- and satellite-based observations to study linkages between terrestrial energy and mass budgets. PhD. Dissertation, School of Forestry, *The University of Montana*, Missoula, MT., 280 pp.

Trenberth, K.E., J. Fasullo, J. Kiehl (2009). Earth's global energy budget. *B. Am. Meteorol. Soc*. 90 (3): 311–323.

Turner, D.P., W.D. Ritts, W.B. Cohen, S.T. Gower, M. Zhao, S.W. Running, et al. (2003a). Scaling gross primary production (GPP) over boreal and deciduous forest landscapes in support of MODIS GPP product validation. *Remote Sensing of Environment*, 88: 256−270.

Turner,D.P., S. Urbanski, D. Bremer, S.C. Wofsy, T. Meyers, S.T. Gower, et al. (2003b). A cross-biome comparison of daily light use efficiency for gross primary production. *Global Change Biology* 9: 383−395.

Tuzet, A., A. Perrier, R. Leuning (2003). Stomatal control of photosynthesis and transpiration: Results from a soil–plant–atmosphere continuum model. *Plant, Cell and Environment*, 26, 1097-1116.

Van de Griend, A. A. (1994). Bare soil surface resistance to evaporation by vapor diffusion under semiarid conditions. *Water Resources Research*, 30, 181−188.

Vickers, D., M. Gockede, B. Law (2010). Uncertainty estimates for 1-hour averaged turbulence fluxes of carbon dioxide, latent heat and sensible heat. *Tellus B*, 62, 87-99.

Vörösmarty, C. J., C.A. Federer, A.L. Schloss (1998). Potential evaporation function compared on US watersheds: Possible implication for global-scale water balance and terrestrial ecosystem. *Journal of Hydrology*, 207: 147−169.

Vörösmarty, C. J., P. B. McIntyre, M. O. Gessner, D. Dudgeon, A. Prusevich, P. Green, S. Glidden, S. E. Bunn, C. A. Sullivan, C. Reidy Liermann, P. M. Davies (2010) Global threats to human water security and river biodiversity. *Nature* 467: 555–561. doi:10.1038/nature09440.

Wallace, J.S., C.J. Holwill (1997). Soil evaporation from Tiger-Bush in South-West Niger. *Journal of Hydrology* 188–189: 426−442.

Wan, Z., Y. Zhang, Q. Zhang, Z.L. Li (2002). Validation of the land-surface temperature products retrieved from Terra Mode rate Resolution Imaging Spectroradiometer data. *Remote Sensing of Environment* 83: 163-180.

Wang, Y., C.E. Woodcock, W. Buermann, P. Sternberg, P. Voipoi, H. Smolander, et al. (2004). Evaluation of the MODIS LAI algorithm at a coniferous forest site in Finland. *Remote Sensing of Environment*, 91, 114−127.

Watkins, A.B. (2005) The Australian drought of 2005. Offprint of an article that appeared in *WMO Bulletin* 54 (3) (July 2005) http://www.geo.uio.no/edc/downloads/the_australian_drought_of_2005_-_offprint_of_wmo_bulletin_2005_54%283%29_156-162.pdf.

Weber, S., A. Graf, B.G. Heusinkveld (2002). Accuracy of soil heat flux plate measurements in coarse substrates - Field measurements versus a laboratory test. *THEOR APPL CLIMATOL* 89 (2007)39479: 109-114.

White, M. A., P. E. Thornton, S. W. Running and R. R. Nemani (2000) Parameterization and Sensitivity Analysis of the BIOME-BGC Terrestrial Ecosystem model: Net Primary Production Controls. *Earth Interactions* 4 (3): 1-85.

Wilson, K., A. Goldstein, E. Falge, M. Aubinet, D. Baldocchi, P. Berbigier, C. Bernhofer, R. Ceulemans, H. Dolman, C. Field, A. Grelle, A. Ibrom, B.E. Law, A. Kowalski, T. Meyers, J. Moncrieff, R. Monson, W. Oechel, J. Tenhunen, R. Valentini, S. Verma (2002). Energy balance closure at FLUXNET sites. Agric. Forest Meteorol. 113: 223–243.

Wood, E.F., H. Su, M. McCabe, Z. Su (2003). Estimating evaporation from satellite remote sensing. Paper presented at the International Geoscience and Remote Sensing Symposium, 21-25 July 2003, Toulouse (PID20004.pdf).

Xia, Y., M. B. Ek, Q. Mu, M. T. Hobbins (2012) Evaluation of NLDAS-2 Evapotranspiration against Tower Flux Site Observations. *Journal of Hydrology* (in revision).

Xu, L., D.D. Baldocchi (2003). Seasonal trend of photosynthetic parameters and stomatal conductance of blue oak (Quercus douglasii) under prolonged summer drought and high temperature. *Tree Physiology* 23, 865-877.

Y. Tian, R.E. Dickinson, L. Zhou, X. Zeng, Y. Dai, R.B. Myneni, Y. Knyazikhin, X. Zhang, M. Friedl, H. Yu, W. Wu, M. Shaikh (2004). Comparison of seasonal and spatial variations of leaf area index and fraction of absorbed photosynthetically active radiation from Moderate Resolution Imaging Spectroradiometer (MODIS) and Common Land Model. *J. Geophys. Res.* 109, D01103.

Yang, W., B. Tan, D. Huang, M. Rautiainen, N.V. Shabanov, Y. Wang, et al. (2006). MODIS leaf area index products: From validation to algorithm improvement. *IEEE Transactions on Geoscience and Remote Sensing*, 44, 1885−1898.

Yi, C., D. Ricciuto, R. Li, X. Xu, et al. (2010). Climate control of terrestrial carbon exchange across biomes and continents. *Environ. Res*. Lett. 5.

Yuan, W.P., S.G. Liu, G.R. Yu, J.M. Bonnefond JM, J.Q. Chen, K. Davis, A.R. Desai, A.H. Goldstein, D. Gianelle, F. Rossi, A.E. Suyker, S.B. Verma (2010). Global estimates of evapotranspiration and gross primary production based on MODIS and global meteorology data. *Remote Sensing of Environment* 114 (7): 1416-1431.

Zeppel, M., D. Tissue, D. Taylor, C. Macinnis-NG, D. Eamus (2010). Rates of nocturnal transpiration in two evergreen temperate woodland species with differing water-use strategies. *Tree Physiology* 30, 988–1000

Zhan, X., W. P. Kustas, K. S. Humes (1996). An intercomparison study on models of sensible heat flux over partial canopy surfaces with remotely sensed surface temperature. *Remote Sensing of Environment* 58: 242-256.

Zhang, K., J.S. Kimball, Q. Mu, L.A. Jones, S. Goetz, S.W. Running (2009). Satellite based analysis of northern ET trends and associated changes in the regional water balance from 1983 to 2005. *Journal of Hydrology* 379: 92-110.

Zhao, M., H.A. Heinsch, R. Nemani, S.W. Running (2005). Improvements of the MODIS terrestrial gross and net primary production global data set. *Remote Sensing of Environment* 95: 164−176.

Zhao, M., S. W. Running (2010). Drought-induced reduction in global terrestrial net primary production from 2000 through 2009. *Science* 329 (5994): 940 – 943.

Zhou, B., L. Gu, Y. Ding, L. Shao, Z. Wu, X. Yang, C. Li, Z. Li, X. Wang, Y. Cao, B. Zeng, M. Yu, M. Wang, S. Wang, H. Sun, A. Duan, Y. An, X. Wang, W. Kong (2010). The Great 2008 Chinese ice storm, its socioeconomic-ecological impact, and sustainability lessons learned. Bulletin of the American Meteorological Society (BAMS); e-View doi: 10.1175/2010BAMS2857.1